

Differentially Private Clustered Federated Learning

Saber Malekmohammadi^{1 2} Afaf Taik² Golnoosh Farnadi^{2 3 4}

Abstract

Federated learning (FL), which is a decentralized machine learning (ML) approach, often incorporates differential privacy (DP) to provide rigorous data privacy guarantees. Previous works attempted to address high *structured* data heterogeneity in vanilla FL settings through clustering clients (a.k.a clustered FL), but these methods remain sensitive and prone to errors, further exacerbated by the DP noise. This vulnerability makes the previous methods inappropriate for differentially private FL (DPFL) settings with structured data heterogeneity. To address this gap, we propose an algorithm for differentially private clustered FL, which is robust to the DP noise in the system and identifies the underlying clients' clusters correctly. To this end, we propose to cluster clients based on both their model updates and training loss values. Furthermore, for clustering clients' model updates at the end of the first round, our proposed approach addresses the server's uncertainties by employing large batch sizes as well as Gaussian Mixture Models (GMM) to reduce the impact of DP and stochastic noise and avoid potential clustering errors. This idea is efficient especially in privacy-sensitive scenarios with more DP noise. We provide theoretical analysis to justify our approach and evaluate it across diverse data distributions and privacy budgets. Our experimental results show its effectiveness in addressing large structured data heterogeneity in DPFL.

1. Introduction

Federated learning (FL) (McMahan et al., 2017) is a collaborative ML paradigm, which allows multiple clients to train a shared global model without sharing their data. However, in order for FL algorithms to ensure rigorous privacy

guarantees against data privacy attacks (Hitaj et al., 2017; Rigaki & García, 2020; Wang et al., 2019; Zhu et al., 2019; Geiping et al., 2020), they are reinforced with DP (Dwork et al., 2006b;a; Dwork, 2011; Dwork & Roth, 2014). This is done in the presence of a trusted server (McMahan et al., 2018; Geyer et al., 2017) as well as its absence (Zhao et al., 2020; Duchi et al., 2013; 2018). In the latter case and for sample-level DP, each client runs DP-SGD (Abadi et al., 2016) locally and shares its noisy model updates with the server at the end of each round.

A key challenge in FL settings is ensuring an acceptable performance across clients under heterogeneous data distributions. Several existing works focus on accuracy parity across clients with a *single* common model by agnostic FL (Mohri et al., 2019) and client reweighting (Li et al., 2020b;a; Zhang et al., 2023). However, a single global model often fails to adapt to the data heterogeneity across clients (Dwork et al., 2012), especially when high data heterogeneity exists. Furthermore, when using a single model and augmenting FL with DP, different subgroups of clients are unevenly affected - even with loose privacy guarantees (Farrand et al., 2020; Fioretto et al., 2022; Bagdasaryan & Shmatikov, 2019). In fact, subgroups with minority clients experience a larger drop in model utility, due to the inequitable gradient clipping in DP-SGD (Abadi et al., 2016; Bagdasaryan & Shmatikov, 2019; Xu et al., 2021; Esipova et al., 2022). Accordingly, some works proposed to use model personalization by multi-task learning (Smith et al., 2017; Li et al., 2021; Marfoq et al., 2021; Wu et al., 2023), transfer learning (Li & Wang, 2019; Liu et al., 2020) and clustered FL (Ghosh et al., 2020; Mansour et al., 2020; Ruan & Joe-Wong, 2021; Sattler et al., 2019; Werner et al., 2023; Briggs et al., 2020). The latter has been proposed for vanilla FL and is suitable when “structured data heterogeneity” exists across clusters of clients (as in this work): subsets of clients can be naturally grouped together based on their data distributions and one model is learned for each group (cluster). However, as discussed in (Werner et al., 2023), the existing non-private clustered FL approaches are vulnerable to errors in clustering due to their sensitivity to: 1. model initialization 2. randomness in clients' model updates due to stochastic noise. The DP noise existing in DPFL systems' training mechanism exacerbates this vulnerability by injecting more randomness.

¹School of Computer Science, University of Waterloo, Waterloo, Canada ²Mila - Quebec AI institute, Montreal, Canada ³School of Computer Science, McGill University, Montreal, Canada ⁴Université de Montréal, Montreal, Canada. Correspondence to: Saber Malekmohammadi <saber.malekmohammadi@uwaterloo.ca>.

To address the aforementioned gap, we propose a differentially private clustered FL algorithm which uses both clients' model updates and loss values for clustering clients, making it more robust to DP/stochastic noise (Algorithm 1): 1) Justified by our theoretical analysis (Lemma 4.1 and 4.2) and in order to cluster clients correctly, our proposed algorithm uses a full batch size in the first FL round and a small batch size in the subsequent rounds, to reduce the noise in clients' model updates at the end of the first round. 2) Then, the server soft clusters clients based on these less noisy model updates using a Gaussian Mixture Model (GMM). Depending on the "confidence" of the learned GMM, the server keeps using it to soft cluster clients during the next few rounds (Section 4.4). 3) Finally, the server switches the clustering strategy to local clustering of clients based on their loss values in the remaining rounds. These altogether make our DP clustered FL algorithm effective and robust. The highlights of our contributions are as follows:

- We propose a DP clustered FL algorithm (R-DPCFL), which combines information from both clients' model updates and their loss values. The algorithm is robust and achieves high-quality clustering of clients, even in the presence of DP noise in the system (Algorithm 1).
- We theoretically prove that increasing clients' batch sizes in the first round (and decreasing them in the subsequent rounds) improves the server's ability to cluster clients based on their model updates at the end of the first round with high accuracy (Lemma 4.2).
- We show that utilizing sufficiently large client batch sizes in the first round (and sufficiently small batch sizes in the next rounds) enables super-linear convergence rate for learning a GMM on clients' model updates at the end of the first round. This leads to soft clustering of clients using a GMM with a low computational overhead (Theorem 4.3).
- We extensively evaluate across diverse datasets and scenarios, and demonstrate the effectiveness of our robust DP clustered FL algorithm in detecting the underlying cluster structure of clients, which leads to an overall utility improvement for the system (Section 5).

2. Related work

Model personalization is a technique for improving utility under moderate data heterogeneity (Li et al., 2021; Liu et al., 2022a), which usually leverages extra computations, e.g., extra local iterations (Li et al., 2021). On the other hand, clustered FL has been proposed for personalized FL with "structured" data heterogeneity, where clients can be naturally partitioned into clusters: clients in the same cluster have similar data distributions, while there is significant

heterogeneity among the various clusters. Existing clustered FL algorithms group clients based on their loss values (Ghosh et al., 2020; Mansour et al., 2020; Ruan & Joe-Wong, 2021; Dwork et al., 2012; Liu et al., 2022b) or their model updates (based on e.g., their euclidean distance (Werner et al., 2023; Briggs et al., 2020) or cosine similarity (Sattler et al., 2019)). As shown by (Werner et al., 2023), the algorithms are prone to clustering errors in the early rounds of FL training –due to gradient stochasticity, model initialization or the form of loss functions far from their optima– which can even propagate in the subsequent rounds. This vulnerability is exacerbated in DPFL systems, due to the existing extra DP noise. Without addressing this vulnerability, (Luo et al., 2024) proposed a DP clustered FL algorithm with a limited applicability, which clusters clients based on the labels that they do not have in their local data. In contrast, our DP clustered FL algorithm is applicable to any setting characterized by a number of clients, where each client holds many data samples and needs sample-level privacy protection. Cross-silo FL systems can be considered as an instance. The closest study to this setting was recently done by (Liu et al., 2022a), which considers silo-specific sample-level DP and studies the interplay between privacy and data heterogeneity. More specifically, they show that when clients have large dataset sizes and under "moderate" data heterogeneity across clients: 1. participation in FL by clients is encouraged over local training, as the model averaging on the server side yields to mitigation of DP noise 2. under the same total privacy budget, model personalization –through mean regularized multi-task learning (MR-MTL)– leads to a better performance compared to learning a single global model or local training by clients (see Appendix D.4 about MR-MTL formulation). Complementing the work, we show that MR-MTL, local training and even loss-based client clustering are not efficient for DPFL with "structured" data heterogeneity across clusters of clients.

3. Definitions, Notations and assumptions

There are multiple definitions of DP. We adopt the following definition to be satisfied by every client:

Definition 3.1 ((ϵ, δ) -DP (Dwork et al., 2006a)). A randomized mechanism $\mathcal{M} : \mathcal{A} \rightarrow \mathcal{R}$ with domain \mathcal{A} and range \mathcal{R} satisfies (ϵ, δ) -DP if for any two adjacent inputs $\mathcal{D}, \mathcal{D}' \in \mathcal{A}$, which differ only by a single record (by replacement), and for any measurable subset of outputs $\mathcal{S} \subseteq \mathcal{R}$ it holds that

$$\Pr[\mathcal{M}(\mathcal{D}) \in \mathcal{S}] \leq e^\epsilon \Pr[\mathcal{M}(\mathcal{D}') \in \mathcal{S}] + \delta.$$

The gaussian mechanism randomizes the output of a query f as $\mathcal{M}(\mathcal{D}) \triangleq f(\mathcal{D}) + \mathcal{N}(0, \sigma^2)$. The randomized output of the mechanism satisfies (ϵ, δ) -DP for a continuum of pairs (ϵ, δ) : it is (ϵ, δ) -DP for all ϵ and $\sigma > \frac{\sqrt{2 \ln(1.25/\delta)}}{\epsilon} \Delta_2 f$, where $\Delta_2 f \triangleq \max_{\mathcal{D}, \mathcal{D}'} \|f(\mathcal{D}) - f(\mathcal{D}')\|_2$ is the l_2 -

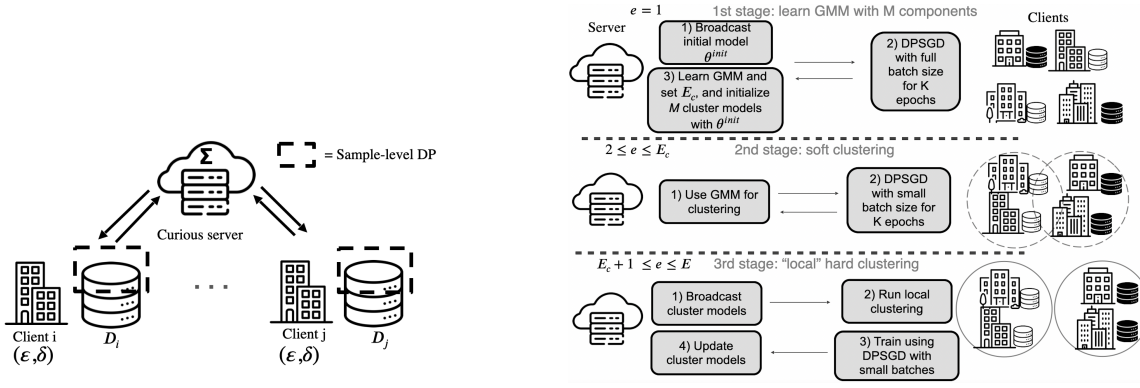


Figure 1. **Left:** Considered threat model in this work, where client i has local train data \mathcal{D}_i and “sample-level” DP privacy parameters (ϵ, δ) , and does not trust any external party. **Right:** Three main stages of the proposed R-DPCFL algorithm.

sensitivity of the query f with respect to its input. Also, the ϵ and δ privacy parameters resulting from running Gaussian mechanism depend on the quantity $z = \frac{\sigma}{\Delta_2 f}$ (called “noise scale”). We consider a DPFL system (see Figure 1, left), where there are n clients running DPSGD with the same “sample-level” privacy parameters (ϵ, δ) : the set of information (including model updates and cluster selections) sent by client i to the server satisfies (ϵ, δ) -DP for all adjacent datasets \mathcal{D}_i and \mathcal{D}'_i of the client i differing in one sample.

Let $x \in \mathcal{X} \subseteq \mathbb{R}^d$ and $y \in \mathcal{Y} = \{1, \dots, C\}$ denote an input data point and its target label. Client i holds dataset \mathcal{D}_i with N_i samples from distribution $P_i(x, y) = P_i(y|x)P_i(x)$. Let $h : \mathcal{X} \times \boldsymbol{\theta} \rightarrow \mathbb{R}^C$ be the predictor function, which is parameterized by $\boldsymbol{\theta} \in \mathbb{R}^p$. Also, let $\ell : \mathbb{R}^C \times \mathcal{Y} \rightarrow \mathbb{R}_+$ be the used loss function (cross-entropy loss). Client i in the system has empirical train loss $f_i(\boldsymbol{\theta}) = \frac{1}{N_i} \sum_{(x,y) \in \mathcal{D}_i} [\ell(h(x, \boldsymbol{\theta}), y)]$, with minimum value f_i^* . There are E communication rounds indexed by e and K local epochs with learning rate η_l during each round. There are M clusters of clients indexed by m , and the server holds M cluster models $\{\boldsymbol{\theta}_m^e\}_{m=1}^M$ for them at the beginning of round e . Clients i and j belonging to the same cluster have the same data distributions, while there is high data heterogeneity across clusters. $s(i)$ denotes the true cluster of client i and $R^e(i)$ denotes the cluster assigned to it at the beginning of round e . Let us assume the batch size used by client i in the first round $e = 1$ is b_i^1 , which may be different from the batch size $b_i^{>1}$ that it uses in the rest of the rounds $e > 1$. At the t -th gradient update during the round e , client i uses batch $\mathcal{B}_i^{e,t}$ with size b_i^e , and computes the following DP noisy batch gradient:

$$\bar{g}_i^{e,t}(\boldsymbol{\theta}) = \frac{1}{b_i^e} \left[\left(\sum_{j \in \mathcal{B}_i^{e,t}} \bar{g}_{ij}(\boldsymbol{\theta}) \right) + \mathcal{N}(0, \sigma_{i,\text{DP}}^2 \mathbb{I}_p) \right], \quad (1)$$

where $\bar{g}_{ij}(\boldsymbol{\theta}) = \text{clip}(\nabla \ell(h(x_{ij}, \boldsymbol{\theta}), y_{ij}), c)$, and c is a clipping threshold to clip sample gradients: for a given vector \mathbf{v} , $\text{clip}(\mathbf{v}, c) = \min\{\|\mathbf{v}\|, c\} \cdot \frac{\mathbf{v}}{\|\mathbf{v}\|}$. Also, \mathcal{N} is the Gaussian noise distribution with variance $\sigma_{i,\text{DP}}^2$, where

$\sigma_{i,\text{DP}} = c \cdot z_i(\epsilon, \delta, b_i^1, b_i^{>1}, N_i, K, E)$, and z_i is the noise scale needed for achieving (ϵ, δ) -DP by client i , which can be determined with a privacy accountant, e.g., Renyi-DP accountant (Mironov et al., 2019) used in this work, which is capable of accounting composition of *heterogeneous* DP mechanisms (Mironov, 2017). The privacy parameter δ is fixed to 10^{-4} in this work and for every client i : $\delta < N_i^{-1}$. For an arbitrary random $\mathbf{v} = (v_1, \dots, v_p)^\top \in \mathbb{R}^{p \times 1}$, we define $\text{Var}(\mathbf{v}) := \sum_{j=1}^p \mathbb{E}[(v_j - \mathbb{E}[v_j])^2]$, i.e., variance of \mathbf{v} is the sum of the variances of its elements. Table 1 in the appendix summarizes the used notations. Finally, we have the following assumption:

Assumption 3.2. The stochastic gradient $g_i^{e,t}(\boldsymbol{\theta}) = \frac{1}{b_i^e} \sum_{j \in \mathcal{B}_i^{e,t}} g_{ij}(\boldsymbol{\theta})$ is an unbiased estimate of $\nabla f_i(\boldsymbol{\theta})$ with a bounded variance: $\forall \boldsymbol{\theta} \in \mathbb{R}^p : \text{Var}(g_i^{e,t}(\boldsymbol{\theta})) \leq \sigma_{i,g}^2(b_i^e)$. The tight bound $\sigma_{i,g}^2(b_i^e)$ is a constant depending only on the used batch size b_i^e : the larger b_i^e , the smaller $\sigma_{i,g}^2(b_i^e)$.

4. Methodology and proposed algorithm

As discussed in (Werner et al., 2023), existing *non-DP* clustered FL algorithms are prone to clustering errors, especially in the first rounds (see Appendix B for a detailed discussion and an illustrating example). Motivated by this vulnerability, which will get exacerbated by DP noise, we next propose a DP clustered FL algorithm which starts with clustering clients based on their model updates for the first several rounds and then switches its strategy to cluster clients based on their loss values. We augment this idea with some other non-obvious techniques to enhance the clustering accuracy.

4.1. R-DPCFL algorithm

Our proposed R-DPCFL algorithm has three main steps (also see Figure 1, right and Algorithm 1):

1. In the first round, clients train the initial model $\boldsymbol{\theta}^{\text{init}}$ locally. They use **full batch sizes** in this round to make

Algorithm 1: R-DPCFL

Input: Initial parameter θ^{init} , dataset sizes $\{N_1, \dots, N_n\}$, batch sizes $\{b_1^{>1}, \dots, b_n^{>1}\}$, clip bound c , local epochs K , global round E , number of clusters M (optional)

Output: cluster models $\{\theta_m^E\}_{m=1}^M$

```

1 for each client  $i \in \{1, \dots, n\}$  do
2    $b_i^1 \leftarrow N_i$ ; // full batch sizes in the first round
3    $z_i \leftarrow \text{RDP}(\epsilon, \delta, b_i^1, b_i^{>1}, N_i, K, E)$ 
4 for  $e \in \{1, \dots, E\}$  do
5   if  $e = 1$  then
6     for each client  $i \in \{1, \dots, n\}$  in parallel do
7        $\Delta \tilde{\theta}_i^1 \leftarrow \text{DPSGD}(\theta^{init}, b_i^1, N_i, K, z_i, c)$ ; // DPSGD with full batch size on  $\theta^{init}$ 
8     on server:
9     if  $M$  is unknown then
10       $M = \arg \max_{M'} \text{MSS}(\text{GMM}(\Delta \tilde{\theta}_1^1, \dots, \Delta \tilde{\theta}_n^1; M'))$ ; // when  $M$  is unknown (Section 4.4)
11       $\{\pi_1, \dots, \pi_n, \text{MPO}\} = \text{GMM}(\Delta \tilde{\theta}_1^1, \dots, \Delta \tilde{\theta}_n^1; M)$ ; // 1st stage: GMM with  $M$  components
12      set  $E_c(\text{MPO})$ ; //  $E_c$  is set based on MPO (Section 4.4)
13      Initialize:  $\theta_1^2 = \dots = \theta_M^2 = \theta^{init}$ ; // initialize the  $M$  cluster models uniformly
14      continue; // go to the next round ( $e = 2$ )
15   else if  $e \in \{2, \dots, E_c\}$  then
16     for each client  $i \in \{1, \dots, n\}$  do
17        $R^e(i) \leftarrow m$  with probability  $\pi_i[m]$ ; // 2nd stage: soft clustering
18   else
19     on server: broadcast cluster models  $\{\theta_m^e\}_{m=1}^M$  to all clients
20     for each client  $i \in \{1, \dots, n\}$  do
21        $R^e(i) = \arg \min_m f_i(\theta_m^e)$ ; // 3rd stage: "local" clustering
22   for each client  $i \in \{1, \dots, n\}$  in parallel do
23      $\Delta \tilde{\theta}_i^e \leftarrow \text{DPSGD}(\theta_{R^e(i)}^e, b_i^{>1}, N_i, K, z_i, c)$ ; // DPSGD with batch size  $b_i^{>1}$  on  $\theta_{R^e(i)}^e$ 
24   on server:
25   for each client  $i \in \{1, \dots, n\}$  do
26      $w_i^e \leftarrow \frac{1}{\sum_{j=1}^n \mathbb{1}_{R^e(j)=R^e(i)}}$ 
27   for  $m \in \{1, \dots, M\}$  do
28      $\theta_m^{e+1} \leftarrow \theta_m^e + \sum_{i \in \{1, \dots, n\}} \mathbb{1}_{R^e(i)=m} w_i^e \Delta \tilde{\theta}_i^e$ ; //  $i$  contributes to  $R^e(i)$ 
    
```

their model updates $\{\Delta \tilde{\theta}_i^1\}_{i=1}^n$ less noisy¹. Then, the server **soft clusters them by learning GMM on their model updates**. The number of clusters (M) is either given or can be found by maximizing the confidence of the learned GMM (Section 4.4).

- During the subsequent rounds $e \in \{2, \dots, E_c\}$, the server uses the learned GMM to **soft-cluster clients**: client i uses a small batch size $b_i^{>1}$ and contributes to the training of each cluster (m) model proportional to the probability of its assignment to that cluster ($\pi_{i,m}$).

¹Note that even when clients have a limited memory budget, they can still perform DPSGD with full batch size and no computational overhead by using gradient accumulation technique (see Appendix D).

The number of rounds E_c is set based on “confidence level” of the learned GMM (Section 4.4).

- After the first E_c rounds, some progress has been made in the training of the cluster models $\{\theta_m^{E_c}\}_{m=1}^M$. Now, clients’ train loss values on cluster models are meaningful and is the right time to **hard cluster clients based on their loss values** during the remaining rounds to build more personalized models per cluster: $R^e(i) = \arg \min_m f_i(\theta_m^e)$.

In Sections 4.2 and 4.3, we provide theoretical justifications and analysis for the proposed method, especially the usage of full batch size in the first round.

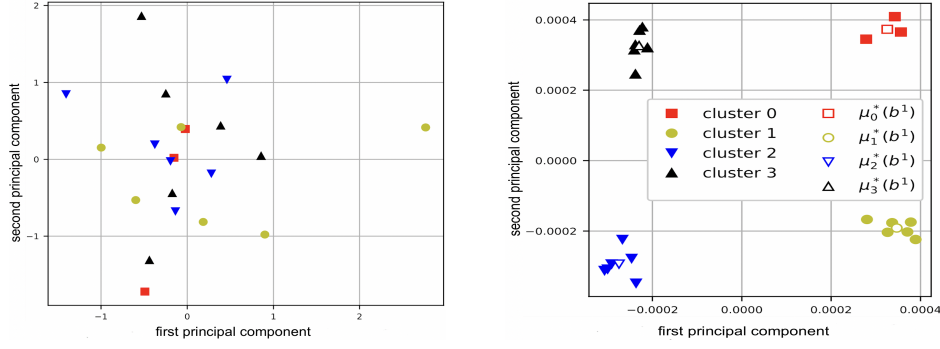


Figure 2. PCA visualization of updates $\{\Delta\tilde{\theta}_i^1\}_{i=1}^n$ on 2D space. **Left:** $\epsilon_i = 10$, $b_i^e = 32$ for all i and e . **Right:** $\epsilon_i = 10$, $b_i^1 = b^1 = N = 6600$, i.e., **full batch sizes** (assuming $N_i = N = 6600$ for all clients), and $b_i^{>1} = 32$ for all i . The empty markers show the centers of the Gaussian components. The model updates are obtained from clients running DP-SGD for $K = 1$ epochs locally on CIFAR10 with covariate shift (rotation) across clusters, and under the same values as in Figure 3.

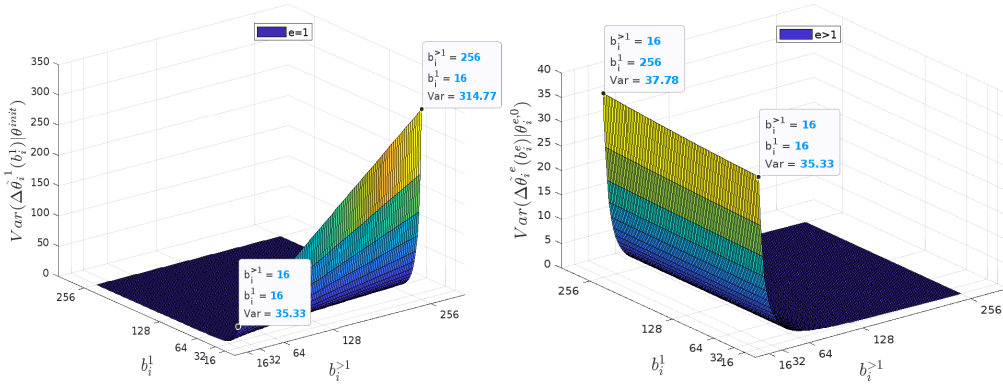


Figure 3. Plot of $\text{Var}(\Delta\tilde{\theta}_i^1(b_i^1)|\theta_i^{init})$ (left) and $\text{Var}(\Delta\tilde{\theta}_i^e(b_i^e)|\theta_i^{e,0})$ ($e > 1$) (right) v.s. both b_i^1 and $b_i^{>1}$. There are two clear takeaways: 1) for all $e \in \{1, \dots, E\}$, $\text{Var}(\Delta\tilde{\theta}_i^e(b_i^e)|\theta_i^{e,0})$ decreases with b_i^e steeply (from Lemma 4.1). 2) The effect of $b_i^{>1}$ on $\text{Var}(\Delta\tilde{\theta}_i^1(b_i^1)|\theta_i^{init})$ (left figure) is considerable. The reason is that $b_i^{>1}$ is used in $E - 1$ rounds and affects the noise scale $z_i(\epsilon, \delta, b_i^1, b_i^{>1}, N_i, K, E)$ used by DP-SGD: see Figure 13 in the appendix for the plot of $z_i(\epsilon, \delta, b_i^1, b_i^{>1}, N_i, K, E)$ v.s. b_i^1 and $b_i^{>1}$. The results are obtained on CIFAR10 from Renyi-DP Accountant (Mironov et al., 2019) in a setting with $N_i = 6600$, $\epsilon = 5$, $\delta = 10^{-4}$, $c = 3$, $K = 1$, $E = 200$, $p = 11, 181, 642$, $\eta_l = 5 \times 10^{-4}$.

4.2. Reducing GMM uncertainty via using full batch sizes in the first round and small batch sizes in the subsequent rounds

The DP noise in $\{\Delta\tilde{\theta}_i^1\}_{i=1}^n$ makes it harder for the server to cluster clients by learning a GMM on the model updates. The following lemma quantifies this noise amount by extending a result in (Malekmohammadi et al., 2024) to when different batch sizes are used in the first and the next rounds:

Lemma 4.1. *Let us assume $\theta_i^{e,0}$ is the model parameter passed to client i at the beginning of round e . After K local epochs with step size η_l , the client generates the noisy DP model update $\Delta\tilde{\theta}_i^e(b_i^e)$ at the end of the round. The amount of noise in the resulting model update can be found as:*

$$\begin{aligned} \sigma_i^{e,2}(b_i^e) &:= \text{Var}(\Delta\tilde{\theta}_i^e(b_i^e)|\theta_i^{e,0}) \\ &\approx K \cdot N_i \cdot \eta_l^2 \cdot \frac{pc^2 z_i^2(\epsilon, \delta, b_i^1, b_i^{>1}, N_i, K, E)}{b_i^{e,3}}. \end{aligned} \quad (2)$$

The first conclusion from the lemma is that the noise level in $\Delta\tilde{\theta}_i^e$ rapidly declines as b_i^e increases: See Figure 3 and the effect of batch size b_i^1 on $\text{Var}(\Delta\tilde{\theta}_i^1|\theta_i^{init})$ (on the left) and the effect of batch size $b_i^{>1}$ on $\text{Var}(\Delta\tilde{\theta}_i^e|\theta_i^{e,0})$ ($e > 1$) (on the right). Let us consider $e = 1$ especially: If all clients use full batch sizes in the first round (i.e., $b_i^1 = N_i$ for every client i), it becomes much easier for the server to cluster them at the end of the first round by learning a GMM on $\{\Delta\tilde{\theta}_i^1\}_{i=1}^n$, as their updates become more separable. An illustration of this is shown in Figure 2. In the next section, we will provide a theoretical justification for this observation. As the second key takeaway, Figure 3, left shows that **in order to make $\{\Delta\tilde{\theta}_i^1\}_{i=1}^n$ less noisy, we have to make $\{b_i^1\}_{i=1}^n$ as large as possible and also keep $\{b_i^{>1}\}_{i=1}^n$ small².**

²In fact, there is a close relation between the result of Lemma 4.1 and the law of large numbers. See Appendix H for more details

4.2.1. EFFECT OF BATCH SIZES $\{b_i^1\}_{i=1}^n$ ON THE SEPARATION BETWEEN CLUSTERS

In this section, we provide a theoretical justification for the observation in Figure 2, right. *For simplicity, let us assume clients have the same dataset sizes and first batch sizes: $\forall i : N_i = N, b_i^1 = b^1$.* Also, remember that $\theta_i^{1,0} = \theta^{init}$. Having uniform privacy parameters (ϵ, δ) , we have: $\forall i : \sigma_i^{1^2}(b^1) := \text{Var}[\Delta\tilde{\theta}_i^1(b^1)|\theta^{init}] = \sigma^{1^2}(b^1)$. Hence, we can consider the model updates $\{\Delta\tilde{\theta}_i^1(b^1)\}_{i=1}^n$ as the samples from a mixture of M Gaussians with mean, covariance matrix, prior probability parameters: $\psi^*(b^1) = \{\mu_m^*(b^1), \Sigma_m^*(b^1), \alpha_m^*\}_{m=1}^M$, where $\forall m : \alpha_m^* > 0$ and $\mu_m^*(b^1) \neq \mu_{m'}^*(b^1)$ ($m \neq m'$), due to data heterogeneity:

$$\mu_m^*(b^1) := \mathbb{E} \left[\Delta\tilde{\theta}_i^1(b_i^1) \middle| \theta^{init}, b_i^1 = b^1, s(i) = m \right], \quad (3)$$

$$\Sigma_m^*(b^1) := \mathbb{E} \left[(\Delta\tilde{\theta}_i^1(b_i^1) - \mu_m^*(b^1)) (\Delta\tilde{\theta}_i^1(b_i^1) - \mu_m^*(b^1))^\top \middle| \theta^{init}, b_i^1 = b^1, s(i) = m \right] = \frac{\sigma^{1^2}(b^1)}{p} \mathbb{I}_p, \quad (4)$$

where the last equality is from $\text{Var}[\Delta\tilde{\theta}_i^1|\theta^{init}, b_i^1 = b^1] = \mathbb{E}[\|\Delta\tilde{\theta}_i^1 - \mu_{s(i)}^*(b^1)\|^2] = \sigma^{1^2}(b^1)$ and that the noises existing in each of the p elements of $\Delta\tilde{\theta}_i^1$ are *i.i.d* (hence, $\Sigma_m^*(b^1)$ is a diagonal covariance matrix with equal diagonal elements). Intuitively, we expect more separation between the true Gaussian components $\{\mathcal{N}(\mu_m^*(b^1), \Sigma_m^*(b^1))\}_{m=1}^M$, from which clients' updates $\{\Delta\tilde{\theta}_i^1\}_{i=1}^n$ are sampled, to make the model updates more distinguishable for server. Next, we show that the overlap between the Gaussian components $\{\mathcal{N}(\mu_m^*(b^1), \Sigma_m^*(b^1))\}_{m=1}^M$ decreases fast with b^1 : **Lemma 4.2.** *Let $\Delta_{m,m'}(b^1) := \|\mu_m^*(b^1) - \mu_{m'}^*(b^1)\|$ when $\forall i : b_i^1 = b^1$. The overlap between components $\mathcal{N}(\mu_m^*(b^1), \Sigma_m^*(b^1))$ and $\mathcal{N}(\mu_{m'}^*(b^1), \Sigma_{m'}^*(b^1))$ is $O_{m,m'} = 2Q(\frac{\sqrt{p}\Delta_{m,m'}(b^1)}{2\sigma^{1^2}(b^1)})$, where $\sigma^{1^2}(b^1) := \text{Var}[\Delta\tilde{\theta}_i^1|\theta^{init}, b_i^1 = b^1]$ and $Q(\cdot)$ is the Q function. Furthermore, if we increase $b_i^1 = b^1$ to $b_i^1 = kb^1 \leq N$ (for all i), we have $O_{m,m'} \leq 2Q(\frac{\sqrt{kp}\Delta_{m,m'}(b^1)}{2\rho\sigma^{1^2}(b^1)})$, where $1 \leq \rho \in \mathcal{O}(1)$ is a small constant.*

Note that for a batch size b^1 , the terms $\Delta_{m,m'}(b^1)$ and $\sigma^{1^2}(b^1)$ represent the “data heterogeneity level across clusters m and m' ” and “privacy sensitivity of their clients”, respectively. We define their “separation score” as $SS(m, m') := \frac{\sqrt{p}\Delta_{m,m'}(b^1)}{2\sigma^{1^2}(b^1)} = \frac{\Delta_{m,m'}(b^1)}{2\sigma^{1^2}(b^1)/\sqrt{p}}$. The larger separation score $SS(m, m')$, the smaller their pairwise overlap $O_{m,m'} = 2Q(SS(m, m'))$. Based on the form of the Q function, an $SS(m, m')$ above 3 can be considered as a complete separation between the corresponding components.

4.3. Convergence rate of EM for learning GMM

Let us define the maximum pairwise overlap between the components in $\psi^*(b^1) = \{\mu_m^*(b^1), \Sigma_m^*(b^1), \alpha_m^*\}_{m=1}^M$, as $O^{\max}(\psi^*(b^1)) = \max_{m,m'} O_{m,m'}(\psi^*(b^1))$. According to Lemma 4.2, when b^1 is large enough, $O^{\max}(\psi^*(b^1))$ decreases (like in Figure 2, right) and we can expect EM to converge to the true GMM parameters $\psi^*(b^1)$. Next, we analyze the local convergence rate of EM around $\psi^*(b^1)$.

Theorem 4.3. (Ma et al., 2000) *Given model updates $\{\Delta\tilde{\theta}_i^1(b^1)\}_{i=1}^n$, as samples from a true mixture of Gaussians $\psi^*(b^1) = \{\mathcal{N}(\mu_m^*(b^1), \Sigma_m^*(b^1)), \alpha_m^*\}_{m=1}^M$, if $O^{\max}(\psi^*(b^1))$ is small enough, then:*

$$\lim_{r \rightarrow \infty} \frac{\|\psi^{r+1} - \psi^*(b^1)\|}{\|\psi^r - \psi^*(b^1)\|} = o\left([O^{\max}(\psi^*(b^1))]^{0.5-\gamma}\right), \quad (5)$$

as n increases. ψ^r is the GMM parameters returned by EM after r iterations. γ is an arbitrary small positive number, and $o(x)$ means it is a higher order infinitesimal as $x \rightarrow 0$: $\lim_{x \rightarrow 0} \frac{o(x)}{x} = 0$.

This means that convergence rate of EM around the true solution $\psi^*(b^1)$ is faster than how $[O^{\max}(\psi^*(b^1))]^{0.5-\gamma}$ decreases with b^1 (from Lemma 4.2). Hence, as an important consequence, the computational complexity of learning the GMM in the first round also decreases fast as b^1 increases.

4.4. Applicability of R-DPCFL

As we observed in Lemma 4.2, the separation score $SS(m, m')$ (the overlap $O_{m,m'}$) increases (decreases) as b^1 increases. Remember that $SS(m, m') = \frac{\Delta_{m,m'}(b^1)}{2\sigma^{1^2}(b^1)/\sqrt{p}}$, and note that $\sigma^{1^2}(b^1)/p$ is the value of diagonal elements of covariance matrices of Gaussian components, which the GMM aims to learn (see Equation (4)). Therefore, when the GMM is learned, we can use its parameters to get an estimate score $\hat{SS}(m, m')$ for every pair of clusters m and m' . Then, we can define the “minimum pairwise separation score” as $\text{MSS}(\epsilon, \delta, \{b_i^1\}_{i=1}^n, \{b_i^{>1}\}_{i=1}^n) = \min_{m,m'} \hat{SS}(m, m') \in [0, +\infty)$ as a **measure of confidence** of the learned GMM in its identified clusters. The larger the MSS of a learned GMM, the more “confident” it is in its clustering decisions. For instance, if we learn a GMM on Figure 2 left, it will have a much smaller MSS than when we learn a GMM on Figure 2 right. We can similarly define the estimated “maximum pairwise overlap” for a learned GMM as $\text{MPO} = 2Q(\text{MSS}) \in [0, 1)$, as a **measure of uncertainty** of the learned GMM. We can use MSS and MPO of the learned GMM to set the switching time E_c , batch sizes $\{b_i^1\}_{i=1}^n$ and even the number of underlying clusters M (when it is unknown). We refer to Appendix E for a detailed explanation.

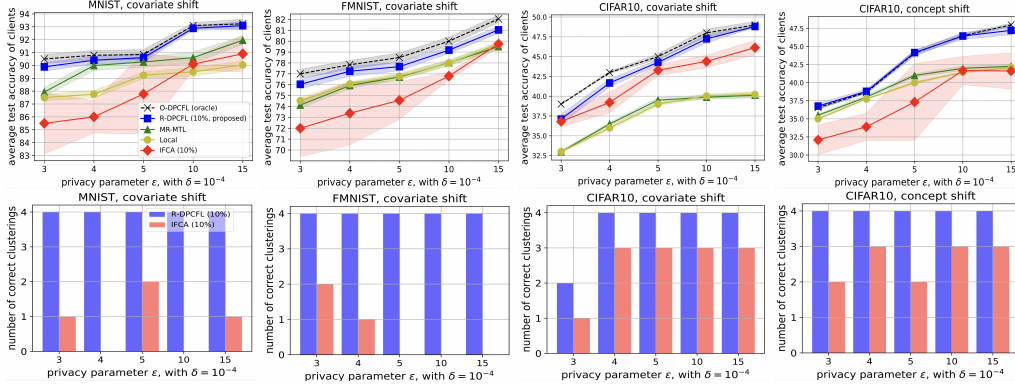


Figure 4. **Top:** Average test accuracy across clients for different total privacy budgets ϵ . Results are from four different runs. 10% means performing local clustering by clients only in 10% of the total number of rounds; i.e., rounds $E_c \leq e \leq E_c + \lfloor \frac{E}{10} \rfloor$ for R-DPCFL and rounds $1 \leq e \leq 1 + \lfloor \frac{E}{10} \rfloor$ for IFCA (see Appendix D.6). **Figure 10 in the appendix includes the Global baseline too.** **Bottom:** Number of times (out of 4 runs) that R-DPCFL and IFCA are successfully detect the underlying cluster structure of all existing clients.

5. Evaluation

Datasets, models and baseline algorithms: We evaluate our proposed method on three benchmark datasets, including: MNIST (Deng, 2012), FMNIST (Xiao et al., 2017) and CIFAR10 (Krizhevsky, 2009), with heterogeneous data distributions from covariate shift (rotation; $P_i(x)$ varies across clusters) (Kairouz et al., 2021; Werner et al., 2023) and concept shift (label flip; $P_i(y|x)$ varies across clusters) (Werner et al., 2023), which are the commonly used data splits for clustered FL (see Appendix D). We consider four clusters of clients indexed by $m \in \{0, 1, 2, 3\}$ with $\{3, 6, 6, 6\}$ clients, where the smallest cluster is considered as the minority cluster. We compare our method with most recent related DPFL algorithms under an equal total sample-level privacy budget ϵ : 1. Global (Noble et al., 2021): clients run DP-SGD locally and send their model updates to the server for aggregation and learning one global model 2. Local (Liu et al., 2022a): clients do not participate FL and learn a local model by running DP-SGD on their local data 3. A DP extension of IFCA (Ghosh et al., 2020; Liu et al., 2022a): local loss/accuracy-based clustering performed by clients on existing cluster models 4. MR-MTL (Liu et al., 2022a): uses model personalization to learn one model for each client 5. O-DPCFL: an oracle algorithm which has the knowledge of the true clusters from the first round. For R-DPCFL and IFCA, we use exponential mechanism (Rogers & Steinke, 2021), which satisfies zero concentrated DP (z-CDP) (Bun & Steinke, 2016), to privatize clients’ local cluster selections.

5.1. Results

Liu et al. (2022a) observed that under sample-level differential privacy and “mild” data heterogeneity, federation is more beneficial than local training, because, despite the data heterogeneity across the clients, the model aggregation (averaging) on the server results in reduction of the DP noise in

clients’ model updates. However, when there is a high structured data heterogeneity across clusters of clients, the level of heterogeneity is remarkable. Hence, learning one global model through FL is not beneficial, as one single model can barely adapt to the high level of data heterogeneity across the clusters. Therefore, in DP clustered FL systems, local training and model personalization can be better options than global training, as they diminish the adverse effect of the high data heterogeneity. Furthermore, *if one can detect the underlying clusters*, one can perform FL in each of them separately and will simultaneously benefit from 1. eliminating the effect of data heterogeneity across clusters; 2. reduction of the DP noise by running FL aggregation on the server within each cluster. Hence, *if the clustering task is done accurately*, we can expect a further improvement over local training and model personalization. This is exactly what R-DPCFL is designed for.

RQ1: How does R-DPCFL perform in practice? Figure 4 shows the average test accuracy across clients for four datasets. As can be observed, R-DPCFL outperforms the baseline algorithms, and this can be attributed to the robust clustering method of R-DPCFL, which additionally benefits from the unused information in clients’ model updates in the first round and leads to correct clustering of clients (Figure 4, bottom row). While R-DPCFL performs close to the oracle algorithm, IFCA has a lower performance due to its errors in detecting the underlying true clusters. For instance, IFCA has a clearly low clustering accuracy on MNIST and FMNIST, which leads it to perform even worse than Local and MR-MTL. In contrast, it has a better clustering performance on CIFAR10 (covariate and concept shifts) and outperforms the two baselines. On the other hand, the reason behind the low performance of MR-MTL is that it performs personalization on a global model, which in turn has a low quality due to being obtained from federation across “all” clients (hence adversely affected by the high data heterogeneity).

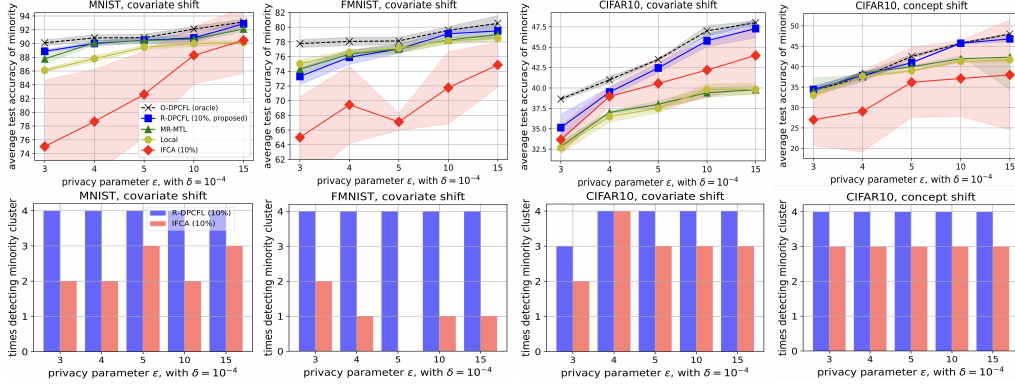


Figure 5. **Top:** Average test accuracy across clients belonging to the minority cluster for different total privacy budgets ϵ , and four different runs. **Bottom:** Number of times (out of 4 runs) that R-DPCFL and IFCA successfully detect the minority cluster.

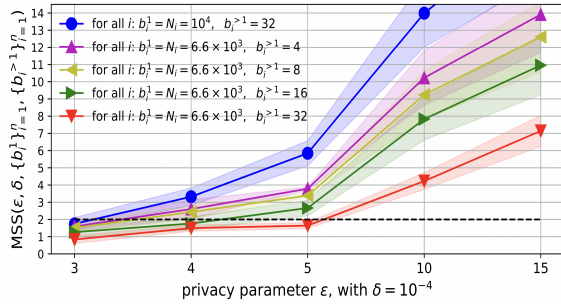


Figure 6. MSS score v.s. ϵ for two different local dataset sizes. A small local dataset size can be compensated for by using smaller batch sizes $\{b_i^{>1}\}_{i=1}^n$ to get a larger MSS score.

Similarly, Local, which performs close to MR-MTL, cannot outperform R-DPCFL, as it does not benefit from the DP noise reduction by FL aggregation within each cluster.

RQ2: How does the minority cluster benefit from R-DPCFL? Figure 5 compares different algorithms based on the average test accuracy of the clients belonging to the minority cluster. R-DPCFL leads to a better overall performance for the minority clients, by virtue of its correct and robust cluster detection. Correct detection of the minority cluster prevents it from getting mixed with other majority clusters and leads to a utility improvement for its clients. In contrast, IFCA has a lower success rate in detecting the minority cluster (Figure 5, bottom row) and provides a lower overall performance for them. Similarly, Local and MR-MTL lead to a low performance for the minority, as they are conditioned on a global model that is learned from federation across all clients and provides a low performance for the minority. Detecting and improving the performance of minority clusters is important, as the different clusters in DP clustered FL systems may not be of the same size, and failure in detecting them correctly leads to low performance for the ones with smaller sizes.

RQ3: What if clients have small local datasets? While we envision the proposed approach being more applicable

to cross-silo FL, where datasets are large, it is still worth exploring how beneficial it can be under scarce local data. In the previous sections, we analyzed the benefits of using a full batch size ($b_i^1 = N_i$) in the first round and found that it leads to a GMM with a higher MSS confidence score. The score of the learned GMM can strongly predict whether the underlying true clusters will be detected: an MSS above 2 almost always yields to correct detection of the underlying clusters (see Figure 12 for experimental results). On the other hand the MSS score depends on four sets of parameters: $\epsilon, \delta, \{b_i^1\}_{i=1}^n$, and $\{b_i^{>1}\}_{i=1}^n$. For fixed (ϵ, δ) , larger $\{b_i^1\}_{i=1}^n$ and smaller $\{b_i^{>1}\}_{i=1}^n$ increase MSS (Lemma 4.1). When we use full batch sizes in the first round, we have $b_i^1 = N_i$ (for all i). Hence, smaller local datasets result in lower confidence in the learned GMM. Nevertheless, this can be compensated for by using even smaller $\{b_i^{>1}\}_{i=1}^n$. Figure 6 compares two different dataset sizes under varying ϵ . As observed, for smaller local dataset sizes, reducing $\{b_i^{>1}\}_{i=1}^n$ can help obtain less noisy model updates $\{\Delta\theta_i^1\}_{i=1}^n$, improve the MSS score of the learned GMM and consequently, enable a successful client clustering.

6. Conclusion

We proposed a DP clustered FL algorithm, which addresses sample-level privacy in FL systems with structured data heterogeneity. By clustering clients based on both their model updates and training loss/accuracy values, and mitigating noise impacts with large initial batch sizes, our approach enhances clustering accuracy and mitigates DP 's disparate impact on utility, all with minimal computational overhead. Moreover, the robustness to noise and easy parameter selection of the proposed approach shows its applicability to DP clustered FL settings. While envisioned for DPFL systems with large local datasets, the method is capable of compensating for moderate dataset sizes by using smaller batch sizes after the first round. In the future, we aim to extend this approach to be suitable for scarce data scenarios, which might be found in cross-device FL settings.

7. Acknowledgement

Funding support for project activities has been partially provided by Canada CIFAR AI Chair, Facebook award, Google award, and MEI award. We also express our gratitude to Compute Canada for their support in providing facilities for our evaluations.

References

- Abadi, M., Chu, A., Goodfellow, I., McMahan, H. B., Mironov, I., Talwar, K., and Zhang, L. Deep learning with differential privacy. In *Proceedings of the 2016 ACM SIGSAC Conference on Computer and Communications Security*, 2016. URL <https://doi.org/10.1145/2976749.2978318>.
- Bagdasaryan, E. and Shmatikov, V. Differential privacy has disparate impact on model accuracy. In *Neural Information Processing Systems*, 2019. URL <https://arxiv.org/abs/1905.12101>.
- Bertsimas, D., Farias, V. F., and Trichakis, N. The price of fairness. *Operations research*, 59(1):17–31, 2011. URL <https://web.mit.edu/dbertsim/www/papers/Fairness/The%20Price%20of%20Fairness.pdf>.
- Billingsley, P. *Probability and Measure*. John Wiley & Sons, Inc., 1995. ISBN 0471007102. URL <https://www.colorado.edu/amath/sites/default/files/attached-files/billingsley.pdf>.
- Briggs, C., Fan, Z., and Andras, P. Federated learning with hierarchical clustering of local updates to improve training on non-iid data, 2020. URL <https://arxiv.org/abs/2004.11791>.
- Bun, M. and Steinke, T. Concentrated differential privacy: Simplifications, extensions, and lower bounds, 2016. URL <https://arxiv.org/abs/1605.02065>.
- Deng, L. The mnist database of handwritten digit images for machine learning research [best of the web]. *IEEE Signal Processing Magazine*, 2012. URL <https://ieeexplore.ieee.org/document/6296535>.
- Dinh, C. T., Tran, N. H., and Nguyen, T. D. Personalized federated learning with moreau envelopes, 2022. URL <https://arxiv.org/abs/2006.08848>.
- Duchi, J. C., Jordan, M. I., and Wainwright, M. J. Local privacy and statistical minimax rates. *2013 51st Annual Allerton Conference on Communication, Control, and Computing (Allerton)*, pp. 1592–1592, 2013. URL <https://api.semanticscholar.org/CorpusID:1597053>.
- Duchi, J. C., Wainwright, M. J., and Jordan, M. I. Minimax optimal procedures for locally private estimation. *Journal of the American Statistical Association*, 113:182 – 201, 2018. URL <https://api.semanticscholar.org/CorpusID:15762329>.
- Dwork, C. A firm foundation for private data analysis. *Commun. ACM*, 2011. URL <https://doi.org/10.1145/1866739.1866758>.
- Dwork, C. and Roth, A. The algorithmic foundations of differential privacy. *Found. Trends Theor. Comput. Sci.*, 2014. URL <https://dl.acm.org/doi/10.1561/04000000042>.
- Dwork, C., Kenthapadi, K., McSherry, F., Mironov, I., and Naor, M. Our data, ourselves: Privacy via distributed noise generation. In *Proceedings of the 24th Annual International Conference on The Theory and Applications of Cryptographic Techniques*, 2006a. URL https://doi.org/10.1007/11761679_29.
- Dwork, C., McSherry, F., Nissim, K., and Smith, A. Calibrating noise to sensitivity in private data analysis. In *Proceedings of the Third Conference on Theory of Cryptography*. Springer-Verlag, 2006b. URL https://doi.org/10.1007/11681878_14.
- Dwork, C., Hardt, M., Pitassi, T., Reingold, O., and Zemel, R. Fairness through awareness. In *Proceedings of the 3rd Innovations in Theoretical Computer Science Conference*, pp. 214–226. Association for Computing Machinery, 2012. URL <https://doi.org/10.1145/2090236.2090255>.
- Esipova, M. S., Ghomi, A. A., Luo, Y., and Cresswell, J. C. Disparate impact in differential privacy from gradient misalignment. *ArXiv*, abs/2206.07737, 2022. URL <https://api.semanticscholar.org/CorpusID:249712405>.
- Evgeniou, T. and Pontil, M. Regularized multi-task learning. *Association for Computing Machinery*, 2004. URL <https://doi.org/10.1145/1014052.1014067>.
- Farrand, T., Mireshghallah, F., Singh, S., and Trask, A. Neither private nor fair: Impact of data imbalance on utility and fairness in differential privacy. *Proceedings of the 2020 Workshop on Privacy-Preserving Machine Learning in Practice*, 2020. URL <https://api.semanticscholar.org/CorpusID:221655207>.
- Fioretto, F., Tran, C., Hentenryck, P. V., and Zhu, K. Differential privacy and fairness in decisions and learning tasks: A survey. In *Proceedings of the Thirty-First International*

- Joint Conference on Artificial Intelligence*. International Joint Conferences on Artificial Intelligence Organization, jul 2022. doi: 10.24963/ijcai.2022/766. URL <https://doi.org/10.24963%2Fijcai.2022%2F766>.
- Geiping, J., Bauermeister, H., Dröge, H., and Moeller, M. Inverting gradients - how easy is it to break privacy in federated learning? *ArXiv*, 2020. URL <https://api.semanticscholar.org/CorpusID:214728347>.
- Geyer, R. C., Klein, T., and Nabi, M. Differentially private federated learning: A client level perspective. *ArXiv*, 2017. URL <https://arxiv.org/pdf/1712.07557.pdf>.
- Ghosh, A., Chung, J., Yin, D., and Ramchandran, K. An efficient framework for clustered federated learning. In Larochelle, H., Ranzato, M., Hadsell, R., Balcan, M., and Lin, H. (eds.), *Advances in Neural Information Processing Systems*, volume 33, pp. 19586–19597. Curran Associates, Inc., 2020. URL https://proceedings.neurips.cc/paper_files/paper/2020/file/e32cc80bf07915058ce90722ee17bb71-Paper.pdf.
- Hanzely, F. and Richtárik, P. Federated learning of a mixture of global and local models, 2021. URL <https://arxiv.org/abs/2002.05516>.
- Hanzely, F., Hanzely, S., Horváth, S., and Richtárik, P. Lower bounds and optimal algorithms for personalized federated learning, 2020. URL <https://arxiv.org/abs/2010.02372>.
- He, K., Zhang, X., Ren, S., and Sun, J. Deep residual learning for image recognition. In *2016 IEEE Conference on Computer Vision and Pattern Recognition (CVPR)*, 2015. URL https://www.cv-foundation.org/openaccess/content_cvpr_2016/papers/He_Deep_Residual_Learning_CVPR_2016_paper.pdf.
- Hitaj, B., Ateniese, G., and Pérez-Cruz, F. Deep models under the gan: Information leakage from collaborative deep learning. *Proceedings of the 2017 ACM SIGSAC Conference on Computer and Communications Security*, 2017. URL <https://api.semanticscholar.org/CorpusID:5051282>.
- Kairouz, P., McMahan, H. B., Avent, B., Bellet, A., Bennis, M., Bhagoji, A. N., Bonawitz, K., Charles, Z., Cormode, G., Cummings, R., et al. Advances and open problems in federated learning. *Foundations and trends in machine learning*, 14(1–2):1–210, 2021. URL <https://arxiv.org/abs/1912.04977>.
- Krizhevsky, A. Learning multiple layers of features from tiny images, 2009. URL <https://www.cs.toronto.edu/~kriz/learning-features-2009-TR.pdf>.
- Lan, T., Kao, D., Chiang, M., and Sabharwal, A. An axiomatic theory of fairness in network resource allocation. In *2010 Proceedings IEEE INFOCOM*, 2010. URL <https://arxiv.org/abs/0906.0557>.
- Li, D. and Wang, J. Fedmd: Heterogenous federated learning via model distillation. *ArXiv*, abs/1910.03581, 2019. URL <https://api.semanticscholar.org/CorpusID:203951869>.
- Li, T., Beirami, A., Sanjabi, M., and Smith, V. Tilted empirical risk minimization. In *International Conference on Learning Representations*, 2020a. URL <https://arxiv.org/abs/2007.01162>.
- Li, T., Sanjabi, M., Beirami, A., and Smith, V. Fair resource allocation in federated learning. In *International Conference on Learning Representations*, 2020b. URL <https://arxiv.org/abs/1905.10497>.
- Li, T., Hu, S., Beirami, A., and Smith, V. Ditto: Fair and robust federated learning through personalization. In Meila, M. and Zhang, T. (eds.), *Proceedings of the 38th International Conference on Machine Learning*, volume 139 of *Proceedings of Machine Learning Research*, pp. 6357–6368. PMLR, 18–24 Jul 2021. URL <https://proceedings.mlr.press/v139/li21h.html>.
- Liu, J. and Talwar, K. Private selection from private candidates, 2018. URL <https://arxiv.org/abs/1811.07971>.
- Liu, Y., Kang, Y., Xing, C., Chen, T., and Yang, Q. A secure federated transfer learning framework. *IEEE Intelligent Systems*, 35:70–82, 2020. URL <https://api.semanticscholar.org/CorpusID:219013245>.
- Liu, Z., Hu, S., Wu, Z. S., and Smith, V. On privacy and personalization in cross-silo federated learning, 2022a. URL <https://arxiv.org/abs/2206.07902>.
- Liu, Z., Hu, S., Wu, Z. S., and Smith, V. On privacy and personalization in cross-silo federated learning, 2022b. URL <https://arxiv.org/abs/2206.07902>.
- Luo, G., Chen, N., He, J., Jin, B., Zhang, Z., and Li, Y. Privacy-preserving clustering federated learning for non-iid data. *Future Generation Computer Systems*, 154:384–395, 2024. URL <https://www.sciencedirect.com/science/article/pii/S0167739X24000050>.

- Ma, J., Xu, L., and Jordan, M. I. Asymptotic convergence rate of the em algorithm for gaussian mixtures. *Neural Computation*, 2000. URL <https://api.semanticscholar.org/CorpusID:10273602>.
- Malekmohammadi, S., Yu, Y., and Cao, Y. Noise-aware algorithm for heterogeneous differentially private federated learning, 2024. URL <https://arxiv.org/abs/2406.03519>.
- Mansour, Y., Mohri, M., Ro, J., and Suresh, A. T. Three approaches for personalization with applications to federated learning, 2020. URL <https://arxiv.org/abs/2002.10619>.
- Marfoq, O., Neglia, G., Bellet, A., Kameni, L., and Vidal, R. Federated multi-task learning under a mixture of distributions. In *Neural Information Processing Systems*, 2021. URL <https://api.semanticscholar.org/CorpusID:236470180>.
- McMahan, B., Moore, E., Ramage, D., Hampson, S., and y Arcas, B. A. Communication-efficient learning of deep networks from decentralized data. In *Artificial intelligence and statistics*, pp. 1273–1282. PMLR, 2017. URL <https://arxiv.org/abs/1602.05629>.
- McMahan, H. B., Ramage, D., Talwar, K., and Zhang, L. Learning differentially private recurrent language models. In *ICLR*, 2018. URL <https://arxiv.org/pdf/1710.06963.pdf>.
- McMahan, H. B., Andrew, G., Erlingsson, U., Chien, S., Mironov, I., Papernot, N., and Kairouz, P. A general approach to adding differential privacy to iterative training procedures, 2019. URL <https://arxiv.org/abs/1812.06210>.
- Mironov, I. Rényi differential privacy. In *2017 IEEE 30th Computer Security Foundations Symposium (CSF)*, pp. 263–275. IEEE, August 2017. doi: 10.1109/csf.2017.11. URL <http://dx.doi.org/10.1109/CSF.2017.11>.
- Mironov, I., Talwar, K., and Zhang, L. Rényi differential privacy of the sampled gaussian mechanism, 2019. URL <https://arxiv.org/abs/1908.10530>.
- Mohri, M., Sivek, G., and Suresh, A. T. Agnostic federated learning. In *International Conference on Machine Learning*, pp. 4615–4625. PMLR, 2019. URL <https://arxiv.org/abs/1902.00146>.
- Noble, M., Bellet, A., and Dieuleveut, A. Differentially private federated learning on heterogeneous data. In *International Conference on Artificial Intelligence and Statistics*, 2021. URL <https://proceedings.mlr.press/v151/noble22a/noble22a.pdf>.
- Papernot, N. and Steinke, T. Hyperparameter tuning with renyi differential privacy, 2022. URL <https://arxiv.org/abs/2110.03620>.
- Pentyala, S., Neophytou, N., Nascimento, A., Cock, M. D., and Farnadi, G. Privfairfl: Privacy-preserving group fairness in federated learning, 2022. URL <https://arxiv.org/abs/2205.11584>.
- Rigaki, M. and García, S. A survey of privacy attacks in machine learning. *ArXiv*, 2020. URL <https://api.semanticscholar.org/CorpusID:220525609>.
- Rogers, R. and Steinke, T. A better privacy analysis of the exponential mechanism, 2021. URL <https://differentialprivacy.org/exponential-mechanism-bounded-range/>.
- Ruan, Y. and Joe-Wong, C. Fedsoft: Soft clustered federated learning with proximal local updating. *CoRR*, abs/2112.06053, 2021. URL <https://arxiv.org/abs/2112.06053>.
- Sattler, F., Müller, K.-R., and Samek, W. Clustered federated learning: Model-agnostic distributed multitask optimization under privacy constraints. *IEEE Transactions on Neural Networks and Learning Systems*, 32:3710–3722, 2019. URL <https://api.semanticscholar.org/CorpusID:203736521>.
- Smith, V., Chiang, C.-K., Sanjabi, M., and Talwalkar, A. Federated multi-task learning. In *Neural Information Processing Systems*, 2017. URL <https://api.semanticscholar.org/CorpusID:3586416>.
- Tran, C., Fioretto, F., and Hentenryck, P. V. Differentially private and fair deep learning: A lagrangian dual approach. *ArXiv*, abs/2009.12562, 2020. URL <https://api.semanticscholar.org/CorpusID:221970859>.
- Wang, Z., Song, M., Zhang, Z., Song, Y., Wang, Q., and Qi, H. Beyond inferring class representatives: User-level privacy leakage from federated learning. *IEEE INFOCOM*, 2019. URL <https://api.semanticscholar.org/CorpusID:54436587>.
- Werner, M., He, L., Karimireddy, S. P., Jordan, M., and Jaggi, M. Provably personalized and robust federated learning, 2023. URL <https://arxiv.org/abs/2306.08393>.
- Wu, Y., Zhang, S., Yu, W., Liu, Y., Gu, Q., Zhou, D., Chen, H., and Cheng, W. Personalized federated learning under mixture of distributions. *ArXiv*, abs/2305.01068, 2023. URL <https://api.semanticscholar.org/CorpusID:258436670>.

- Xiao, H., Rasul, K., and Vollgraf, R. Fashion-mnist: a novel image dataset for benchmarking machine learning algorithms. *CoRR*, 2017. URL <http://arxiv.org/abs/1708.07747>.
- Xu, D., Du, W., and Wu, X. Removing disparate impact on model accuracy in differentially private stochastic gradient descent. *Proceedings of the 27th ACM SIGKDD Conference on Knowledge Discovery & Data Mining*, 2021. URL <https://api.semanticscholar.org/CorpusID:236980106>.
- Zhang, G., Malekmohammadi, S., Chen, X., and Yu, Y. Proportional fairness in federated learning. *Transactions on Machine Learning Research*, 2023. URL <https://openreview.net/forum?id=ryUHgEdWCQ>.
- Zhao, Y., Zhao, J., Yang, M., Wang, T., Wang, N., Lyu, L., Niyato, D. T., and Lam, K.-Y. Local differential privacy-based federated learning for internet of things. *IEEE Internet of Things Journal*, 8:8836–8853, 2020. URL <https://api.semanticscholar.org/CorpusID:215828540>.
- Zhu, L., Liu, Z., and Han, S. Deep leakage from gradients. In *Neural Information Processing Systems*, 2019. URL <https://api.semanticscholar.org/CorpusID:195316471>.

Appendix for *Differentially Private Clustered Federated Learning*

A. Notations

Table 1 summarizes the notations used in the paper.

Table 1. Used notations

n	number of clients, which are indexed by i
x_{ij}, y_{ij}	j -th data point of client i and its label
\mathcal{D}_i, N_i	local train set of client i and its size
$\mathcal{D}_{i,aug}$	augmented local train set of client i
$\mathcal{B}_i^{e,t}$	the train data batch used by client i in round e and at the t -th gradient update
b_i^e	batch size of client i in round e : $ \mathcal{B}_i^{e,t} = b_i^e$
b_i^1	batch size of client i in the first round $e = 1$
$b_i^{>1}$	set of batch sizes of client i in the rounds $e > 1$
ϵ, δ	desired DP privacy parameters
E	total number of global communication rounds in the DPFL system, indexed by e
θ_m^e	model parameter for cluster m , at the beginning of global round e
K	number of local train epochs performed by clients during each global round e
η	the common learning rate used for DP-SGD
h	predictor function, e.g., CNN model, with parameter θ
ℓ	cross entropy loss
$s(i)$	the true cluster of client i
$R^e(i)$	the cluster assigned to client i in round e
$\theta_i^{e,0}$	the model parameter passed to client i at the beginning of round e to start its local training
$\Delta \tilde{\theta}_i^e$	the noisy model update of client i at the end of round e , starting from $\theta_i^{e,0}$
$\sigma_i^{e,2}$	conditional variance of the noisy model update $\Delta \tilde{\theta}_i^e$ of client i : $\text{Var}(\Delta \tilde{\theta}_i^e \theta_i^{e,0})$
$\mu_m^*(b^1)$	the center of the m -th cluster (when all clients use batch size b^1 in the first round)
$\Sigma_m^*(b^1)$	the covariance matrix of the m -th cluster (when all clients use batch size b^1 in the first round)
α_m^*	the prior probability of the m -th cluster

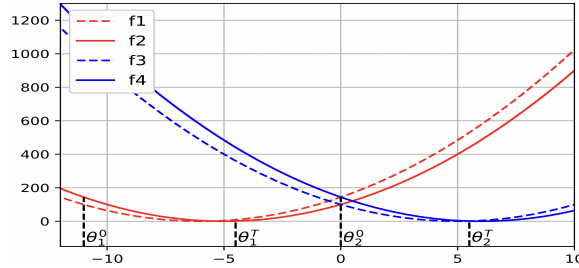


Figure 7. Loss-based clustering algorithms miscluster in the initial rounds, due to model initialization. Also, even with the assumption of perfect clustering of clients in the first rounds, clustering algorithms based on gradients (model updates) lead to clustering errors in the last rounds, due to the gradients approaching to zero.

B. Vulnerability of existing clustered FL algorithms

As discussed in (Werner et al., 2023), clustered FL algorithms which cluster clients based on their loss values (Mansour et al., 2020; Ghosh et al., 2020; Ruan & Joe-Wong, 2021), i.e., assign client i to cluster $R^e(i) = \arg \min_m f_i(\theta_m^e)$ at the beginning of round e , are prone to clustering errors in the first few rounds, mainly due to random initialization of cluster models $\{\theta_m^e\}_{m=1}^M$. On the other hand, clustering clients based on their model updates (gradients) (Werner et al., 2023; Briggs et al., 2020; Sattler et al., 2019) makes sense only when the updates are obtained on the same model initialization. Additionally, even if we assume these algorithms can initially cluster clients perfectly in each round e , the clients' model

updates (gradients) will approach zero as the clusters' models converge to their optimum parameters. Hence, clients from different clusters may appear to belong to the same cluster, which results in clustering mistakes.

We now provide an example to elaborate that why clustering clients based on their losses (model updates) is prone to errors in the first (last) rounds. For example, consider Figure 7, where there are $M = 2$ clusters (red and blue) and $n = 4$ clients. The clients in the red cluster have loss functions $f_1(\theta) = 4(\theta + 6)^2$ and $f_2(\theta) = 4(\theta + 5)^2$ with optimum cluster parameter $\theta_1^\infty = -5.5$. Also, the clients in the blue cluster have loss functions $f_3(\theta) = 4(\theta - 5)^2$ and $f_4(\theta) = 4(\theta - 6)^2$ with optimum cluster parameter $\theta_2^\infty = 5.5$. Clustering algorithms, which cluster clients based on their loss values on clusters' models, are vulnerable to model initialization. For example, in Figure 7, if we initialize the clusters' parameters with $\theta_1^0 = -11$ and $\theta_2^0 = 0$ (shown in the figure), all four clients will initially select cluster 2, since they have smaller losses on its parameter. At $\theta_2^0 = 0$, the average of clients' gradients (model updates) is zero, so all clients will remain stuck at θ_2^0 and will always select cluster 2.

On the other hand, clustering clients based on their model updates (gradients) (Werner et al., 2023; Briggs et al., 2020; Sattler et al., 2019) have clearly issues. One of these issues appears after some rounds of training. For instance, even if we assume these algorithms can initially cluster clients "perfectly" in each round e , the clients' model updates (gradients) will approach zero as the clusters' models converge to their optimum parameters. Hence, clients from different clusters may appear to belong to the same cluster, which results in clustering mistakes. For example, as shown in Figure 1, right, let us assume after T rounds of "correct" clustering of clients, the clusters' parameters get to $\theta_1^T = -4.5$ and $\theta_2^T = 5.5$ (shown in the figure). At this parameters, clients 1 and 2 (which have been "correctly" assigned to cluster 1 so far) will have gradients $f'_1(\theta_1^T) = 12$ and $f'_2(\theta_1^T) = 4$. Similarly, clients 3 and 4 (which have been "correctly" assigned to cluster 2 so far) will have $f'_3(\theta_2^T) = 4$ and $f'_4(\theta_2^T) = -4$. We see that f'_2 is closer to f'_3 and f'_4 than to f'_1 , and in the next round it will wrongly be assigned to wrong cluster 2. This happens while the clients are clearly distinguishable based on their losses, as some progress in training has been made after T rounds: $f_1(\theta_1^T) = 9$, while $f_1(\theta_2^T) = 23^2$, which clearly means that client 1 correctly belongs to cluster 1. Therefore, after making some progress in training the clusters' models, it makes more sense to use a loss-based clustering strategy than using a strategy based on clients' gradients (model updates).

C. Background

C.1. Renyi Differential Privacy (RDP)

We have used a relaxation of Differential Privacy, named Renyi DP (RDP) for tight privacy accounting of different algorithms (Mironov, 2017). It is defined as follows:

Definition C.1 (Renyi Differential Privacy (RDP) (Mironov, 2017)). *A randomized mechanism $\mathcal{M} : \mathcal{A} \rightarrow \mathcal{R}$ with domain \mathcal{D} and range \mathcal{R} satisfies (α, ϵ) RDP with order $\alpha > 1$ if for any two adjacent inputs $\mathcal{D}, \mathcal{D}' \in \mathcal{A}$, which differ only by a single record,*

$$D_\alpha(\mathcal{M}(\mathcal{D}) || \mathcal{M}(\mathcal{D}')) \leq \epsilon,$$

where $D_\alpha(P || Q)$ is the Renyi divergence between distributions P and Q :

$$D_\alpha(P || Q) := \frac{1}{\alpha - 1} \log \mathbb{E}_{x \sim P} \left[\left(\frac{P(x)}{Q(x)} \right)^{\alpha - 1} \right] \quad (\alpha > 1). \quad (6)$$

For $\alpha = 1$, we have $D_1(P || Q) := \mathbb{E}_{x \sim P} \left[\log \left(\frac{P(x)}{Q(x)} \right) \right]$, which is the KL divergence between P and Q . RDP can be used for composition of private mechanisms: if an algorithm has E steps and each step satisfies (α, ϵ) -RDP, the algorithm satisfies $(\alpha, E\epsilon)$ -RDP. RDP can also be used for composition of heterogeneous private mechanisms, e.g., for accounting privacy of R-DPCFL, which uses different batch sizes in the first and next rounds. The following lemma is about conversion of (α, ϵ) -RDP to standard (ϵ, δ) -DP (Definition 3.1).

Lemma C.2. *If a mechanism \mathcal{M} satisfies $(\alpha, \epsilon(\alpha))$ -RDP, then for any $\delta > 0$, it satisfies $(\epsilon(\delta), \delta)$ -DP, where*

$$\epsilon(\delta) = \inf_{\alpha > 1} \epsilon(\alpha) + \frac{1}{\alpha - 1} \log \left(\frac{1}{\alpha \delta} \right) + \log \left(1 - \frac{1}{\alpha} \right). \quad (7)$$

Some accounting routines have been implemented in open source libraries for accounting privacy of RDP mechanisms. We use TensorFlow Privacy implementation (McMahan et al., 2019) in this work.

C.2. Zero Concentrated Differential Privacy (Z-CDP)

Another relaxed definition of differential privacy is zero concentrated differential privacy (z-CDP) (Bun & Steinke, 2016). Being ρ -zCDP is equivalent to being $(\alpha, \rho\alpha)$ -RDP simultaneously for all $\alpha > 1$. Therefore, standard RDP accountants, e.g. the aforementioned TensorFlow Privacy RDP accountant (McMahan et al., 2019), can be used for accounting mechanism satisfying zCDP as well.

C.3. Exponential Mechanism for Private Selection

Exponential Mechanism is a standard for private selection from a set of candidates. The selection is based on a score, which is assigned to every candidate (Rogers & Steinke, 2021). Let us assume there is a private dataset \mathcal{D} and a score function $s : \mathcal{D} \times [M] \rightarrow \mathbb{R}$, which evaluates a set of M candidates on the dataset \mathcal{D} . The goal is to select the candidate with the highest score, i.e., $\arg \max_{m \in [M]} s(\mathcal{D}, m)$. Exponential mechanism performs this selection privately as follows. It sets the probability of choosing any candidate $m \in [M]$ as:

$$\Pr[m] = \frac{\exp(\frac{\epsilon_{\text{select}}}{2\Delta} \cdot s(\mathcal{D}, m))}{\sum_{m' \in [M]} \exp(\frac{\epsilon_{\text{select}}}{2\Delta} \cdot s(\mathcal{D}, m'))}, \quad (8)$$

where δ is the sensitivity of the scoring function s to the replacement of a data sample in \mathcal{D} . It can be shown that the private selection performed by exponential mechanism satisfies $\frac{1}{8}\epsilon_{\text{select}}^2$ -zCDP with respect to \mathcal{D} (Bun & Steinke, 2016), which from the last paragraph, we know satisfies $(\alpha, \frac{\alpha}{8}\epsilon_{\text{select}}^2)$ -RDP for $\alpha > 1$. We implement exponential mechanism by noisy selection with Gumbel noise: we add independent noises from Gumbel distribution with scale $\frac{2\Delta}{\epsilon_{\text{select}}}$ to candidate scores $s(\mathcal{D}, m)$, for $m \in [M]$, and select the candidate with the maximum noisy score. The larger the sensitivity Δ of score s to replacement of a single sample in \mathcal{D} , the required larger noise scale. For further details about how we implement exponential mechanism for IFCA and R-DPCFL, see Appendix D.6.

C.4. Privacy Budgeting

In order to have a fair comparison between our algorithm and the baselines, we align them all to have the same “total” privacy budget ϵ and satisfy (ϵ, δ) -DP for a fixed δ . In order to account the privacy of an algorithm, we compose the RDP guarantees of all private operations in the algorithm and then convert the resulting RDP guarantee to approximate (ϵ, δ) -DP using Lemma C.2. The DP-SGD performed by different algorithms for local training benefits from privacy amplification by subsampling (Mironov et al., 2019). Algorithms that have privacy overheads, e.g., IFCA and R-DPCFL which need to privatize their local clustering as well, will have less privacy budget left for training. In other words, for the same total privacy budget ϵ , IFCA and R-DPCFL will use a larger amount of noise when running DP-SGD, compared to MR-MTL that has zero privacy overhead.

D. Experimental setup

D.1. Datasets

Data split: We use three datasets MNIST, FMNIST and CIFAR10, and consider a distributed setting with 21 clients. In order to create majority and minority clusters, we consider 4 clusters with different number of clients $\{3, 6, 6, 6\}$ (21 clients in total). The first cluster with the minimum number of clients is the “minority” cluster, and the last three are the “majority” ones. The data distribution $P(x, y)$ varies across clusters. We use two methods for making such data heterogeneity: 1. **covariate shift** 2. **concept shift**. In covariate shift, we assume that features marginal distribution $P(x)$ differs from one cluster to another cluster. In order to create this variation, we first allocate samples to all clients in an *uniform* way. Then we rotate the data points (images) belonging to the clients in cluster k by $k * 90$ degrees. For concept shift, we assume that conditional distribution $P(y|x)$ differs from one cluster to another cluster, and we first allocate data samples to clients in a uniform way, and flip the labels of the points allocated to clients: we flip y_{ij} (label of the j -th data point of client i , which belongs to cluster k) to $(y_{ij} + k) \bmod 10$. The local datasets are balanced—all users have the same amount of training samples. The local data is split into train and test sets with ratios 80%, and 20%, respectively. In the reported experimental

results, all users participate in each communication round.

Table 2. CNN model for classification on MNIST/FMNIST datasets

Layer	Output Shape	# of Trainable Parameters	Activation	Hyper-parameters
Input	(1, 28, 28)	0		
Conv2d	(16, 28, 28)	416	ReLU	kernel size =5; strides=(1, 1)
MaxPool2d	(16, 14, 14)	0		pool size=(2, 2)
Conv2d	(32, 14, 14)	12,832	ReLU	kernel size =5; strides=(1, 1)
MaxPool2d	(32, 7, 7)	0		pool size=(2, 2)
Flatten	1568	0		
Dense	10	15,690	ReLU	
Total		28,938		

D.2. Models and optimization

We use a simple 2-layer CNN model with ReLU activation, the detail of which can be found in Table 2 for MNIST and FMNIST. Also, we use the residual neural network (ResNet-18) defined in (He et al., 2015), which is a large model. To update the local models allocated to each client during each round, we apply DPSGD (Abadi et al., 2016) with a noise scale z which depends on some parameters, as in Equation (2).

Table 3. Details of the used datasets in the main body of the paper. ResNet-18 is the residual neural networks defined in (He et al., 2015). CNN: Convolutional Neural Network defined in Table 2.

Datasets	Train set size	Test set size	Data Partition method	# of clients	Model	# of parameters
MNIST	48000	12000	covariate shift	{3, 6, 6, 6}	CNN	28,938
FMNIST	48000	12000	covariate shift	{3, 6, 6, 6}	CNN	28,938
CIFAR10	40000	10000	covariate and concept shift	{3, 6, 6, 6}	ResNet-18	11,181,642

In order to simulate a FL setting, where clients (silos) have large local datasets and there is a structured data heterogeneity across clusters, we split the full dataset between the clients belonging to each cluster. This way, each client gets 8,000 train and 1,666 test samples for MNIST and FMNIST. Also, each client gets 10,000 and 1,666 train and test samples for CIFAR10 dataset (both covariate shift and concept shift).

D.3. Baseline selection

When extending existing model personalization and clustered FL algorithms to DPFL settings, we are mostly interested in those with little to no additional local dataset queries to prevent extra noise for DPSGD under a fixed total privacy budget ϵ . For instance, the family of mean-regularized multi-task learning methods (MR-MTL) (Evgeniou & Pontil, 2004; Hanzely et al., 2020; Hanzely & Richtárik, 2021; Dinh et al., 2022) provide model personalization *without an additional privacy overhead*. Despite this, it is noteworthy that MR-MTL relies on optimal hyperparameter tuning which leads to a potential privacy overhead (Liu et al., 2022a; Liu & Talwar, 2018; Papernot & Steinke, 2022). While resembling MR-MTL, Ditto (Li et al., 2021) has extra local computations, which makes it a less attractive personalization algorithm. Hence, we adopt MR-MTL (Liu et al., 2022a) as a baseline personalization algorithm. Similarly, multi-task learning algorithms of (Smith et al., 2017) and (Marfoq et al., 2021) as well as gradient-based clustered FL algorithm of (Sattler et al., 2019) benefit from additional training and training restarts, which lead to high privacy overhead for them, making them less attractive. In contrast, the aforementioned loss-based clustered FL algorithms (Mansour et al., 2020; Ghosh et al., 2020; Ruan & Joe-Wong, 2021) can be managed to have a low privacy overhead (see Appendix D.6), and we use it as a clustered DPFL baseline.

D.4. MR-MTL formulation

The objective function of Mean-Regularized Multi-Task Learning (MR-MTL) can be expressed as:

$$\min_{\theta_i, i \in \{1, \dots, n\}} \sum_{i=1}^n g_i(\theta_i) \quad \text{with} \quad g_i(\theta_i) = f_i(\theta_i) + \frac{\lambda}{2} \|\theta_i - \bar{\theta}\|_2^2, \quad (9)$$

where $\bar{\theta} = \frac{1}{n} \sum_{i=1}^n \theta_i$ is the average model parameter across clients and $f_i(\theta_i)$ is the loss function of personalized model parameter θ_i of client i on its local dataset \mathcal{D}_i . With $\lambda = 0$, MR-MTL reduces to local training. A larger regularization term λ encourages local models to be closer to each other. However, MR-MTL may not recover FedAvg (McMahan et al., 2017) as $\lambda \rightarrow \infty$. See section E.2 and algorithm A1 in (Liu et al., 2022a) for more details about MR-MTL.

D.5. Tuning hyperparameters of baseline algorithms

Appendix D.3 explains our criteria for baseline selection. We compare our R-DPCFL algorithm, which benefits from robust clustering, with four baseline algorithms, including: 1) DPFedAvg (Noble et al., 2021), which learns one global model for all clients, and is called Global in the paper 2) Local, in which clients do not participate FL and run DP-SGD locally to train a model solely on their local dataset 3) MR-MTL personalized FL algorithm (Liu et al., 2022a), which learns a global model and one personalized model for each client 4) A DP extension of the clustered FL algorithm IFCA (Ghosh et al., 2020) to DPFL systems enhanced with exponential mechanism (see Appendix D.6) 5) An oracle algorithm, which has the knowledge of the true underlying clients’ clusters, which we call O-DPCFL.

For all algorithms and all datasets, we set total number of rounds E to 200 and per-round number of local epochs K to 1. Following (Abadi et al., 2016), we set the batch size of each client such that the number of batches per epoch is in the same order as the total number of epochs: $N_i/b_i^e = E \cdot K = 200$. For MNIST and FMNIST, this leads to batch sizes $b_i^e = 32$ for all clients i and every round e for the baseline algorithms. For CIFAR10 (covariate shift and concept shift), this leads to batch size $b_i^e = 64$ for all clients i and every round e for the baseline algorithms. While R-DPCFL uses full batch sizes in the first round (i.e., $b_i^1 = N_i$ for all i), it needs to use small batch sizes in the next rounds. We have further explained about this in Appendix E.

Having determined the batch size for all algorithms, clipping threshold c and learning rate η_l are determined via a grid search on clients’ validation sets. For each algorithm and each dataset, we find the best learning rate from a grid: the one which results in the highest average accuracy at the end of FL training on a “validation set” with size 1666 samples for each client. We use the grid $\eta_l \in \{5e-4, 1e-3, 2e-3, 5e-3, 1e-2, 2e-2, 5e-2, 1e-1\}$ for all datasets and all algorithms. Similarly, we use the grid $c \in \{1, 2, 3, 4, 5\}$ for setting the clipping threshold for all datasets and all algorithms based on the clients’ validation sets.

D.6. Implementation of private local clustering for IFCA and R-DPCFL

In every round of IFCA and during the rounds $e > E_c$ of R-DPCFL, the server sends M cluster models to all clients, and they evaluate them on their local datasets. Then, each client i selects the model with the lowest loss on its local dataset \mathcal{D}_i , trains it for K local epochs and sends the result back to the server. This model selection performed by each client can lead to privacy leakage w.r.t its local dataset, if it is not privatized. In order to protect data privacy, clients need to privatize their local clustering by using exponential mechanism and accounting its privacy using z-CDP, explained in Appendix C.3. Assuming a total privacy budget ϵ for a client i , it has to split the budget between private clustering and DP-SGD. Naive split of privacy budget can lead to very noisy DP-SGD steps or very noisy local selection by clients. Following (Liu et al., 2022a), we use two strategies to mitigate the privacy overhead of local clustering performed by IFCA and R-DPCFL:

- **Clients use model accuracy, instead of loss, as the score function for model selection:** clients use model accuracy as score function $s(\mathcal{D}_i, m)$ evaluating cluster model m on client i ’s dataset. The reason is that while, loss function has practically an unbounded sensitivity to individual samples in the clients’ datasets, model accuracy is a low-sensitivity function, especially in cross-silo FL settings with large local datasets. More specifically, let us assume client i with local dataset \mathcal{D}_i (which has size N_i) uses models’ accuracy on \mathcal{D}_i for model selection. It can be shown that under all add/remove/replace notions of dataset neighborhood, sensitivity of model accuracy (as score function) is bounded as follows (Liu et al., 2022a):

$$\Delta_{acc} = \max_{m \in [M]} \max_{\mathcal{D}_i, \mathcal{D}'_i} |s(\mathcal{D}_i, m) - s(\mathcal{D}'_i, m)| \leq \frac{1}{N_i - 1}. \quad (10)$$

Since local dataset sizes are usually large, especially in cross-silo FL, the sensitivity of model accuracy is much smaller than that of model loss. Therefore, following (Liu et al., 2022a), we set the per-round privacy budget of private model selection to a very small value $\epsilon_{\text{select}} = 0.03 \cdot \epsilon$ (3% of the total privacy budget). Yet, the cost of private selection by clients can grow quickly if clients naively run local clustering for “many” rounds. Therefore, we use the following strategy as well. It is noteworthy that in our experiments, we observed that IFCA baseline algorithm performs better when clients use model train accuracy (instead of train loss) for cluster selection.

- **Reduce the number of rounds with local clustering on clients’ side:** Clients run local clustering for less rounds. Following (Liu et al., 2022a), we let clients run local clustering for the 10% of the total number of rounds E . For example, IFCA runs local clustering during the first $\lfloor \frac{E}{10} \rfloor$ rounds, and fixes clients’ cluster assignments afterwards. Similarly, R-DPCFL lets clients run local clustering during rounds $E_c \leq e \leq E_c + \lfloor \frac{E}{10} \rfloor$, and fixes clients’ cluster assignments afterwards.

The privacy overhead of private model selection can still grow and leave a low privacy budget for training with DP-SGD. Choosing a small selection budget ϵ_{select} leaves most of the total privacy budget ϵ for training with DP-SGD, but leads to noisy and inaccurate cluster selection by clients. Similarly, a large ϵ_{select} leads to more noisy gradient steps by DP-SGD.

D.7. DP privacy parameters

For each dataset, 5 different values of ϵ (the total privacy budget) from set $\{3, 4, 5, 10, 15\}$ are used. We fix δ for all experiments to 10^{-4} , which satisfies $\delta < N_i^{-1}$ for every client i . We use the Renyi DP (RDP) privacy accountant (TensorFlow privacy implementation (McMahan et al., 2019)) during the training time. This accountant is able to handle the difference in the batch size of R-DPCFL between the first round $e = 1$ and the next rounds $e > 1$ by accounting the composition of the corresponding *heterogeneous* private mechanisms.

D.8. Gaussian Mixture Model

We use the Gaussian Mixture Model of Scikitlearn, which can be found here: <https://scikit-learn.org/dev/modules/generated/sklearn.mixture.GaussianMixture.html>. The GMM model has three hyperparameters:

- 1) parameter initialization, which we set to “k-means++”. This is because this type of initialization leads to both low time to initialize and low number of EM iterations for the GMM to converge
- 2) Type of the covariance matrix, which we set to “spherical”, i.e., each component has a diagonal covariance matrix with a single value as its diagonal elements. This is in accordance with Equation (24) and that we know the covariance matrices should be diagonal.
- 3) Finally, the number of components (clusters) is either known or it is unknown. In the latter case, we have explained in Appendix E.3 how we can find the true number of clusters by using the confidence level (MSS) of the GMM model.

E. Setting hyper-parameters of R-DPCFL

As explained in the paper, R-DPCFL has three hyperparameters, which we explain how to set in the following:

E.1. Batch size $b_i^{>1}$

Batch size $b_i^{>1}$, which is the batch size used by R-DPCFL during the rounds $e > 1$, has to be set to a small value, as observed in Figure 3 right. R-DPCFL is not sensitive to this parameter, as long as a small value is chosen for it. For the results in the paper, we use $b_i^{>1} = 32$ for all experiments with R-DPCFL. We further explain about the effect of this parameter as follows:

As we observed in Lemma 4.1 and Figure 3 left, $\text{Var}(\Delta \tilde{\theta}_i^1(b_i^1) | \theta^{init})$ is an increasing function of $b_i^{>1}$. More generally, the effect of increasing $b_i^{>1}$ is on three things: 1) increasing noise variance $\text{Var}(\Delta \tilde{\theta}_i^1(b_i^1) | \theta^{init})$ (as shown in Figure 3,

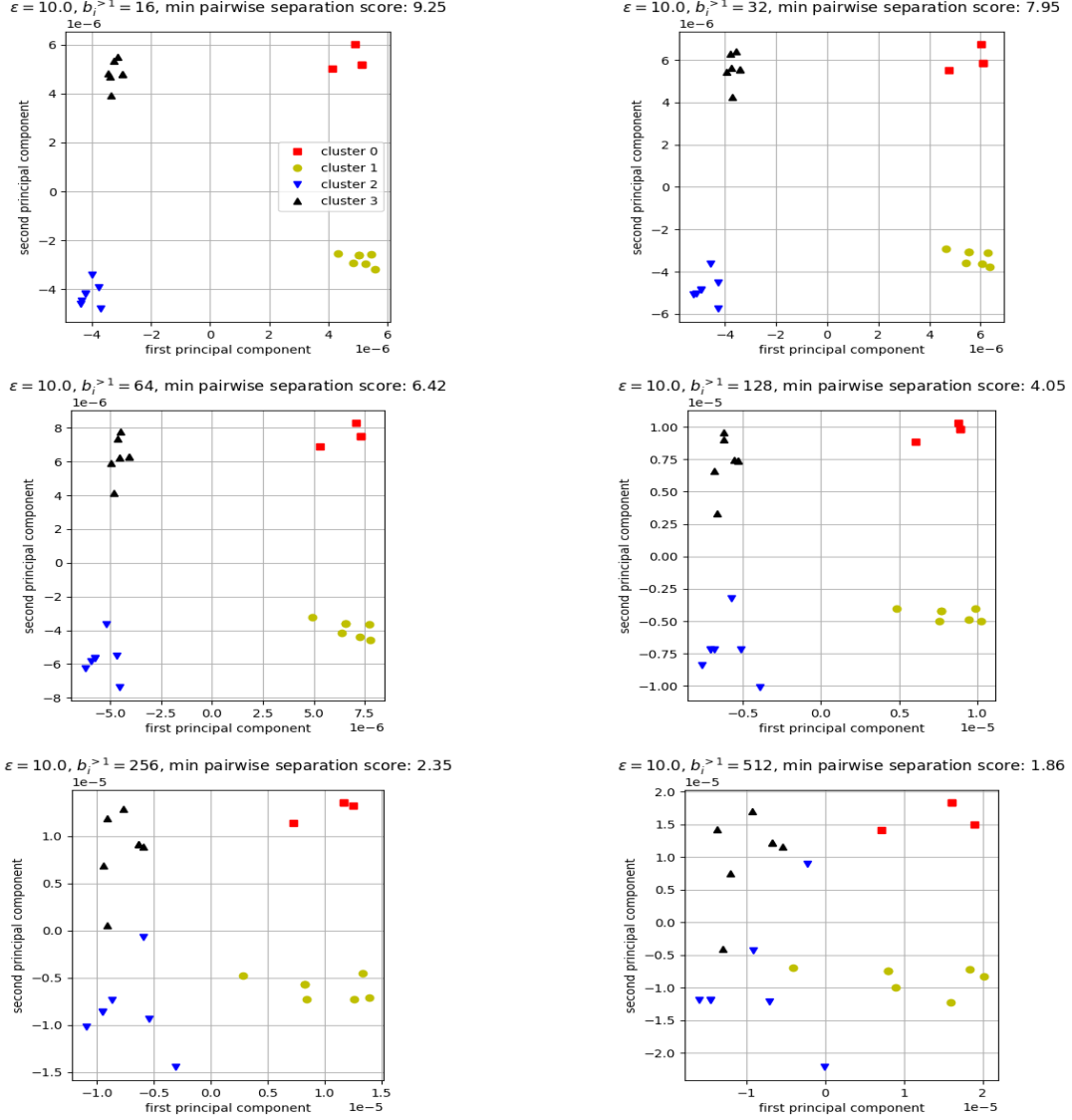


Figure 8. The effect of increasing the batch size after the first round, i.e., $b_i^{>1}$, on the model updates $\{\Delta\hat{\theta}_i^1\}_{i=1}^n$ at the end of the first round. All clients have used full batch sizes in the first round, i.e., $\forall i : b_i^1 = N_i$. The level of noise in $\{\Delta\hat{\theta}_i^1\}_{i=1}^n$ affects the quality and confidence of the client clustering that the server performs at the end of the first round. As can be observed, for a fixed $\epsilon = 10$, the model updates scatter further in space as $b_i^{>1}$ increases and different clusters get less separated. This leads to a decrement in the confidence level or the (MSS) score of the resulting GMM, as $b_i^{>1}$ increases (mentioned on the top of each plot). All the results are obtained on CIFAR10 with covariate shift (rotation) across clusters.

left) 2) decreasing noise variance $\text{Var}(\Delta\tilde{\theta}_i^1(b_i^e)|\theta_i^{e,0})$ (as shown in Figure 3, right) 3) decreasing number of gradient steps during each round e for $e > 1$. While the first one is only limited to the first round $e = 1$, the last two affect the remaining $E - 1$ rounds and have conflicting effects on the final accuracy. However, an important point about the problem of DP clustered FL is that finding the true structure of clusters in the first round is a prerequisite for making progress in the next rounds. Therefore, increment in noise variance $\text{Var}(\Delta\tilde{\theta}_i^1(b_i^1)|\theta^{init})$ (the first effect) is the most important one. We have demonstrated this effect in Figure 8, which shows that how increasing $b_i^{>1}$ adversely affects the clustering done at the end of the first round. Note how MSS score of the learned GMM increases as $b_i^{>1}$ increases. Therefore, in order to have a reliable client clustering at the end of the first round, we need to keep the value of $b_i^{>1}$ to small values: the smaller total privacy budget ϵ , the smaller value should be used for $b_i^{>1}$. Following this observation, we have fixed $b_i^{>1}$ to 32 in all our experiments with R-DPCFL.

E.2. The strategy switching time E_c

The strategy switching time E_c can also be set by using the uncertainty metric $\text{MPO} \in [0, 1)$. Intuitively, if the learned GMM is not certain about its clustering decisions, R-DPCFL should not rely on its decisions for a large E_c , and vice versa. Hence, we can set E_c as a decreasing function of MPO. For instance, $E_c = (1 - \text{MPO})\frac{E}{2}$, which is used in this work, means that if a GMM is completely confident about its clusterings, e.g., what happens in Figure 2 right, the server changes the clustering strategy to loss-based after the first half of rounds. As the uncertainty increases, this change happens earlier (e.g., when ϵ is small), and R-DPCFL slowly gets close to the existing loss-based clustering methods like IFCA (Ghosh et al., 2020).

E.3. The number of clusters M

Knowing the number of clusters is broadly accepted and applied in the clustered FL literature (Ghosh et al., 2020; Ruan & Joe-Wong, 2021; Briggs et al., 2020). **This is the assumption of our baseline algorithms too.** Yet, techniques to determine the number of clusters can enable our approach to be more widely adopted. In this section, we show that how we can find the true number of clusters (M) when it is not given. Our method relies on the MSS score (confidence level) defined in Section 4.4: $\text{MSS} = \min_{m,m'} \hat{S}(m,m') \in [0, +\infty)$ (please see the detailed explanations in Section 4.4). Consider the Figure 2 right as an example. There is a good separation between the $M = 4$ existing clusters, thanks to clients using full batch sizes in the first round. Fitting a GMM with 4 components to the model updates results in the highest MSS for the learned GMM model: remember that MSS was the maximum pairwise separation score between the different components of the learned GMM. In contrast, if we fit a GMM with 3 components (less than the true number of components) to the same model updates in the figure, then two clusters will be merged into one component (for examples clusters 0 and 1) leading to a high radius for one of the three components of the resulting GMM. This leads to a low MSS (confidence level) for the resulting GMM. Similarly, if we fit a GMM with 5 components, one of the four clusters (for example cluster 1) will be split between two of the 5 components (call them m and m'), which leads to a low inter-component distance ($\Delta_{m,m'}$) for the pair of components. This also leads to a low MSS for the resulting GMM. However, **fitting a GMM with $M = 4$ components leads to a well separation between all the true components and maximizes the resulting MSS.** Based on this very intuitive observation, we propose the following method for setting m at the end of the first round: We select the number of clusters/components, which leads to the maximum MSS for the resulting GMM. More specifically:

$$M = \arg \max_{m \in S} \text{MSS}(\text{GMM}(\Delta\tilde{\theta}_1^1, \dots, \Delta\tilde{\theta}_n^1; m)), \text{ (line 9 of Algorithm 1)} \quad (11)$$

where S is a set of candidate values for M : at the end of the first round and on the server, we learn one GMM for each candidate value in S on the same received model updates $\{\Delta\tilde{\theta}_i^1\}_{i=1}^n$. Finally, we choose the value resulting in the GMM with the highest MSS (confidence). Therefore, this method is run on the server and does not incur any additional privacy overheads. It is also noteworthy that we know from Lemma 4.2 that learning the GMM does not incur much computational cost when large enough (and small enough) batch sizes are used in the first round (subsequent rounds).

We have evaluated this method on multiple data splits and different privacy budgets (ϵ) on CIFAR10, MNIST and FMNIST. The method could predict the number of underlying clusters with 100% accuracy for the MNIST and FMNIST datasets for all values of ϵ . Results for CIFAR10 are shown in Figure 9. As can be observed, the method has made only one mistake for $\epsilon = 4$ (seed 1) and two mistakes for $\epsilon = 3$ (seeds 0 and 1), out of 20 total experiments. Even in those three cases, it has predicted M as 5, which is closest to the true value ($M = 4$) and does not lead to much performance drop (because having $M = 5$ splits an existing cluster into two and it is better than predicting for example $M = 3$, which results in "mixing"

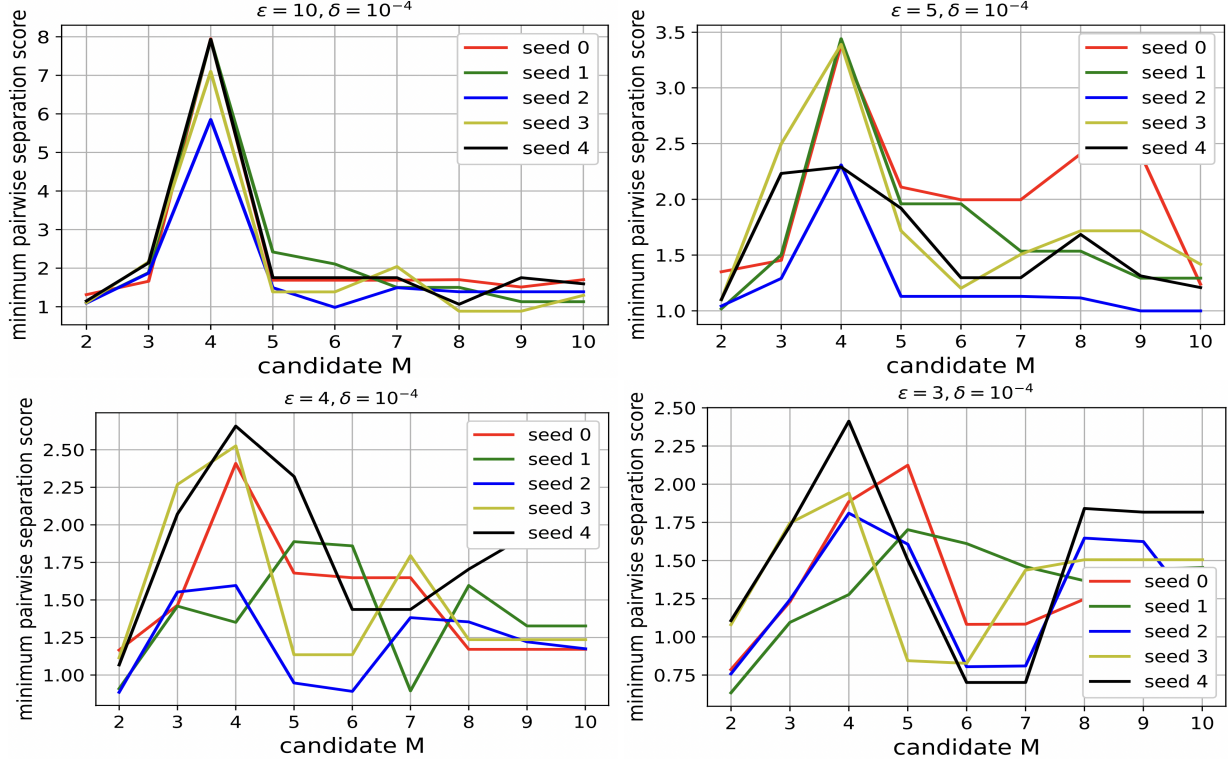


Figure 9. The minimum pairwise separation score (MSS) or confidence of the GMM learned on $\{\Delta\tilde{\theta}_i^1\}_{i=1}^n$ peaks at the true cluster number, which is equal to 4 in all the plots above. Each figure is for a different value of ϵ (mentioned on top of each figure), and are obtained on CIFAR10 with covariate shift (rotation) across clusters, and 5 different random data splits (5 seeds). All the results are obtained with full batch sizes in the first round and $b_i^{>1} = 32$ for all i . We can use this observation as a method to find the true number of clusters (M) when it is not given. For larger ϵ , this method work perfectly and even when ϵ is too small, e.g., $\epsilon = 3$, this method works well and predicts the true number of clusters correctly most of the times: 3 out of the 5 curves in the bottom right plot have a peak at $M = 4$ (the true cluster number), and the other 2 curves predict 5 as the true number, which is the closest and the best alternative for the true value $M = 4$.

two clusters with heterogeneous data). Even in this cases, we can improve the prediction accuracy further by using smaller values of $b_i^{>1}$ (simultaneously with full batch sizes $b_i^1 = N_i$), e.g., $b_i^{>1} = 16$ or $b_i^{>1} = 8$, instead of $b_i^{>1} = 32$ in the figure above. This improvement happens as reducing $b_i^{>1}$ constantly enhances the separation between the underlying components (See Figure 8), which leads to higher accuracy in prediction of the true M .

Finally, note that none of the existing baseline algorithms has such an easy and applicable strategy for finding M . This shows another useful feature of the proposed R-DPCFL, which makes it more applicable to DP clustered FL settings.

F. Complete experimental results

The following figures, which include the results for the Global baseline, are the more complete versions of the figures in the paper (Figure 4 and Figure 5).

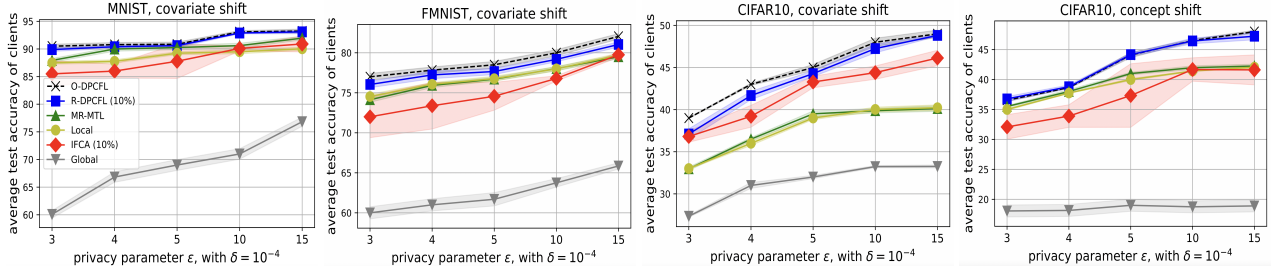


Figure 10. Average test accuracy across clients for different total privacy budgets ϵ (results are obtained from 4 different random seeds). 10% means performing loss-based clustering by clients only in 10% of the total rounds (E).

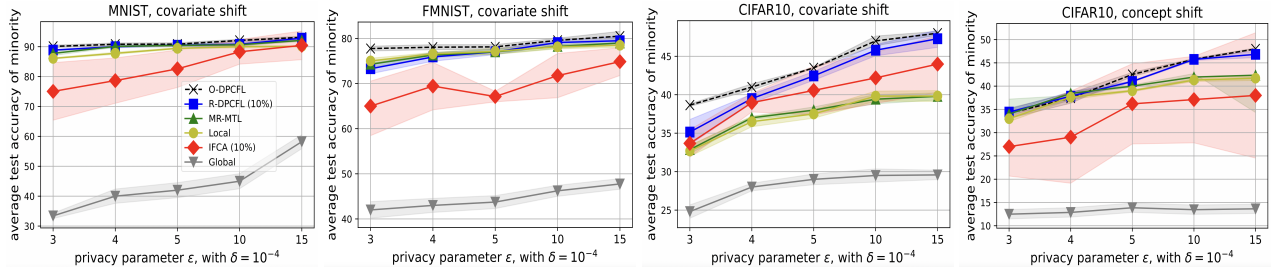


Figure 11. Average test accuracy across clients belonging to the minority cluster for different total privacy budgets ϵ (results are obtained from 4 different random seeds). 10% means performing loss-based clustering by clients only in 10% of the total rounds (E).

The following figure shows how the MSS score of the learned GMM model at the end of the first round can be indicative of whether the true clients' clusters will be detected or not. As observed, an MSS score above 2 almost always yields to correct detection of all clusters.

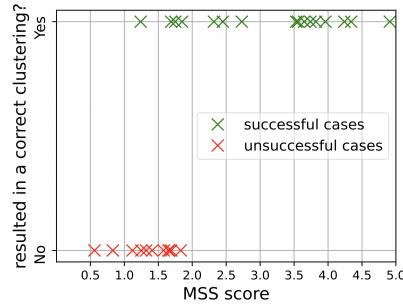


Figure 12. The MSS score of the learned GMM is indicative of whether the true underlying clusters will be detected or not: an MSS score above 2 always leads to correct detection of clusters. Each point is the result of one independent experiment.

G. Proofs

G.1. Proof of Lemma 4.1

Lemma 4.1. *Let us assume $\theta_i^{e,0}$ is the model parameter passed to client i at the beginning of round e . After K local epochs with step size η_l , the client generates the noisy DP model update $\Delta\tilde{\theta}_i^e(b_i^e)$ at the end of the round. The amount of noise in the resulting model update can be found as:*

$$\begin{aligned}\sigma_i^{e^2}(b_i^e) &:= \text{Var}(\Delta\tilde{\theta}_i^e(b_i^e)|\theta_i^{e,0}) \\ &\approx K \cdot N_i \cdot \eta_l^2 \cdot \frac{pc^2 z_i^2(\epsilon, \delta, b_i^1, b_i^{>1}, N_i, K, E)}{b_i^{e^3}}.\end{aligned}\quad (2)$$

Proof. The following proof has some common parts with similar results in (Malekmohammadi et al., 2024). We consider two illustrative scenarios:

Scenario 1: the clipping threshold c is effective for all samples in a batch: in this case we have: $\forall j \in \mathcal{B}_i^{e,t} : c < \|g_{ij}(\theta)\|$. Also, we know that the two sources of randomness (i.e. stochastic and Gaussian noise) are independent, thus their variances can be summed up. Let us assume that $E[\bar{g}_{ij}(\theta)] = G_i(\theta)$ for all samples j . From Equation (1), we can find the mean of each *batch gradient* $\tilde{g}_i^{e,t}(\theta)$ (of client i in round e and gradient step t) as follows:

$$\mathbb{E}[\tilde{g}_i^{e,t}(\theta)] = \frac{1}{b_i^e} \sum_{j \in \mathcal{B}_i^{e,t}} \mathbb{E}[\bar{g}_{ij}(\theta)] = \frac{1}{b_i^e} \sum_{j \in \mathcal{B}_i^{e,t}} G_i(\theta) = G_i(\theta). \quad (12)$$

Also, from Equation (1), we can find the variance of each *batch gradient* $\tilde{g}_i^{e,t}(\theta)$ (of client i in round e and gradient step t) as follows:

$$\begin{aligned}\sigma_{i,\tilde{g}}^2(b_i^e) &:= \text{Var}[\tilde{g}_i^{e,t}(\theta)] = \text{Var}\left[\frac{1}{b_i^e} \sum_{j \in \mathcal{B}_i^{e,t}} \bar{g}_{ij}(\theta)\right] + \frac{p\sigma_{i,\text{DP}}^2}{b_i^{e^2}} \\ &= \frac{1}{b_i^{e^2}} \left(\mathbb{E}\left[\left\|\sum_{j \in \mathcal{B}_i^{e,t}} \bar{g}_{ij}(\theta)\right\|^2\right] - \left\|\mathbb{E}\left[\sum_{j \in \mathcal{B}_i^{e,t}} \bar{g}_{ij}(\theta)\right]\right\|^2 \right) + \frac{pc^2 z_i^2(\epsilon_i, \delta_i, b_i^1, b_i^{>1}, N_i, K, E)}{b_i^{e^2}} \\ &= \frac{1}{b_i^{e^2}} \left(\mathbb{E}\left[\left\|\sum_{j \in \mathcal{B}_i^{e,t}} \bar{g}_{ij}(\theta)\right\|^2\right] - \left\|\sum_{j \in \mathcal{B}_i^{e,t}} G_i(\theta)\right\|^2 \right) + \frac{pc^2 z_i^2(\epsilon_i, \delta_i, b_i^1, b_i^{>1}, N_i, K, E)}{b_i^{e^2}} \\ &= \frac{1}{b_i^{e^2}} \left(\underbrace{\mathbb{E}\left[\left\|\sum_{j \in \mathcal{B}_i^{e,t}} \bar{g}_{ij}(\theta)\right\|^2\right]}_{\mathcal{A}} - b_i^{e^2} \|G_i(\theta)\|^2 \right) + \frac{pc^2 z_i^2(\epsilon_i, \delta_i, b_i^1, b_i^{>1}, N_i, K, E)}{b_i^{e^2}},\end{aligned}\quad (13)$$

where:

$$\begin{aligned}\mathcal{A} &= \mathbb{E}\left[\left\|\sum_{j \in \mathcal{B}_i^{e,t}} \bar{g}_{ij}(\theta)\right\|^2\right] = \sum_{j \in \mathcal{B}_i^{e,t}} \mathbb{E}\left[\|\bar{g}_{ij}(\theta)\|^2\right] + \sum_{m \neq n \in \mathcal{B}_i^{e,t}} 2\mathbb{E}\left[\bar{g}_{im}(\theta)^\top \bar{g}_{in}(\theta)\right] \\ &= \sum_{j \in \mathcal{B}_i^{e,t}} \mathbb{E}\left[\|\bar{g}_{ij}(\theta)\|^2\right] + \sum_{m \neq n \in \mathcal{B}_i^{e,t}} 2\mathbb{E}\left[\bar{g}_{im}(\theta)\right]^\top \mathbb{E}\left[\bar{g}_{in}(\theta)\right] \\ &= b_i^e c^2 + 2 \binom{b_i^e}{2} \|G_i(\theta)\|^2.\end{aligned}\quad (14)$$

The last equation has used Equation (12) and that we clip the norm of sample gradients $\bar{g}_{ij}(\theta)$ with an “effective” clipping threshold c . By replacing \mathcal{A} into eq. 13, we can rewrite it as:

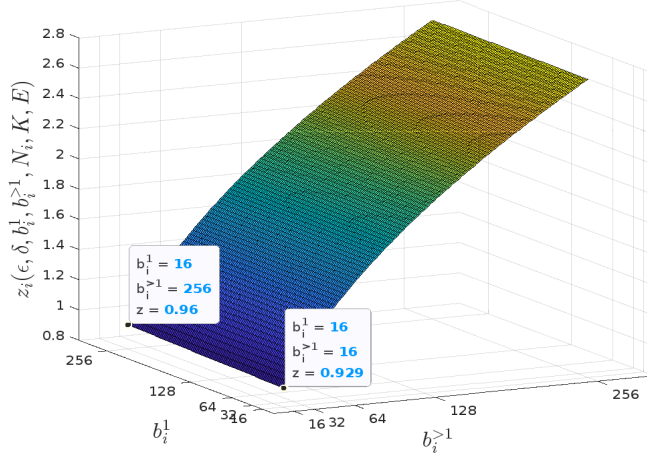


Figure 13. Plot of $z_i(\epsilon, \delta, b_i^1, b_i^{>1}, N_i, K, E)$ v.s. b_i^1 and $b_i^{>1}$ obtained from Renyi-DP Accountant (Mironov et al., 2019) in a setting with $N_i = 6600, \epsilon = 5, \delta = 10^{-4}, K = 1, E = 200$. It is clearly observed that the effect of $b_i^{>1}$ is much more than the effect of b_i^1 . The reason is that $b_i^{>1}$ is used in $E - 1$ rounds, while b_i^1 is used only in the first round. So it is the value of $b_i^{>1}$ that affects z_i the most.

$$\begin{aligned}
 \sigma_{i,\tilde{g}}^2(b_i^e) &:= \text{Var}[\tilde{g}_i^{e,t}(\theta)] = \frac{1}{b_i^{e^2}} \left(\mathbb{E} \left[\left\| \sum_{j \in \mathcal{B}_i^{e,t}} \tilde{g}_{ij}(\theta) \right\|^2 \right] - b_i^{e^2} \|G_i(\theta)\|^2 \right) + \frac{pc^2 z_i^2(\epsilon_i, \delta_i, b_i^1, b_i^{>1}, N_i, K, E)}{b_i^{e^2}} \\
 &= \frac{1}{b_i^{e^2}} \left(b_i^e c^2 + \left(2 \binom{b_i^e}{2} - b_i^{e^2} \right) \|G_i(\theta)\|^2 \right) + \frac{pc^2 z_i^2(\epsilon_i, \delta_i, b_i^1, b_i^{>1}, N_i, K, E)}{b_i^{e^2}} \\
 &= \frac{c^2 - \|G_i(\theta)\|^2}{b_i^e} + \frac{pc^2 z_i^2(\epsilon_i, \delta_i, b_i^1, b_i^{>1}, N_i, K, E)}{b_i^{e^2}} \approx \frac{pc^2 z_i^2(\epsilon_i, \delta_i, b_i^1, b_i^{>1}, N_i, K, E)}{b_i^{e^2}}
 \end{aligned} \tag{15}$$

The last approximation is valid because $p \gg 1$ (it is the number of model parameters).

Scenario 2: the clipping threshold c is ineffective for all samples in a batch: when the clipping is ineffective for all samples, i.e., $\forall j \in \mathcal{B}_i^{e,t} : c > \|g_{ij}(\theta)\|$, we have a noisy version of the batch gradient $g_i^{e,t}(\theta) = \frac{1}{b_i^e} \sum_{j \in \mathcal{B}_i^{e,t}} g_{ij}(\theta)$, which is unbiased with variance bounded by $\sigma_{i,g}^2(b_i^e)$ (see Assumption 3.2). We note that $\sigma_{i,g}^2(b_i^e)$ is a constant that depends on the used batch size b_i^e . The larger the batch size b_i^e used during round e , the smaller the constant. Hence, in this case:

$$\mathbb{E}[\tilde{g}_i^{e,t}(\theta)] = \mathbb{E}[g_i^{e,t}(\theta)] = \nabla f_i(\theta), \tag{16}$$

and

$$\begin{aligned}
 \sigma_{i,\tilde{g}}^2(b_i^e) &= \text{Var}[\tilde{g}_i^{e,t}(\theta)] = \text{Var}[g_i^{e,t}(\theta)] + \frac{p\sigma_{i,\text{DP}}^2}{b_i^{e^2}} \leq \sigma_{i,g}^2(b_i^e) + \frac{p\sigma_{i,\text{DP}}^2}{b_i^{e^2}} \\
 &= \sigma_{i,g}^2(b_i^e) + \frac{pc^2 z_i^2(\epsilon, \delta, b_i^1, b_i^{>1}, N_i, K, E)}{b_i^{e^2}} \\
 &\approx \frac{pc^2 z_i^2(\epsilon, \delta, b_i^1, b_i^{>1}, N_i, K, E)}{b_i^{e^2}}.
 \end{aligned} \tag{17}$$

The approximation is valid because $p \gg 1$ (number of model parameters). Also, note that $\sigma_{i,g}^2(b_i^e)$ decreases with b_i^e . Therefore, we got to the same result as in Equation (15).

As observed in see Figure 13, z_i grows with b_i^1 and $b_i^{>1}$ *sub-linearly* (especially with b_i^1). Therefore, the variance of the client i 's DP batch gradients $\tilde{g}_i^{e,t}(\theta)$ during communication round e , decreases with b_i^e fast. The larger the batch size b_i^e , the less the noise existing in its batch gradients during the same round.

With the findings above, we now investigate the effect of batch size b_i^e on **the noise level in clients' model updates at the end of round e** . During the global communication round e , a participating client i performs $E_i^e = K \cdot \lceil \frac{N_i}{b_i^e} \rceil$ batch gradient updates locally with step size η_l :

$$\theta_i^{e,k} = \theta_i^{e,k-1} - \eta_l \tilde{g}_i(\theta_i^{e,k-1}), \quad k = 1, \dots, E_i^e. \quad (18)$$

Hence,

$$\Delta \tilde{\theta}_i^e = \theta_i^{e,E_i^e} - \theta_i^{e,0} \quad (19)$$

In each update, it adds a Gaussian noise from $\mathcal{N}(0, \frac{c^2 z_i^2(\epsilon, \delta, b^1, b^{>1}, N_i, K, E)}{b_i^{e^2}} \mathbb{I}_p)$ to its batch gradients independently (see Equation (1)). Hence:

$$\text{Var}[\Delta \tilde{\theta}_i^e | \theta_i^{e,0}] = E_i^e \cdot \eta_l^2 \cdot \sigma_{i,\tilde{g}}^2(b_i^e), \quad (20)$$

where $\sigma_{i,\tilde{g}}^2(b_i^e)$ was computed in Equation (15) and Equation (17), and was a decreasing function of b_i^e . Therefore:

$$\text{Var}[\Delta \tilde{\theta}_i^e | \theta_i^{e,0}] \approx K \cdot N_i \cdot \eta_l^2 \cdot \frac{pc^2 z_i^2(\epsilon, \delta, b_i^1, b_i^{>1}, N_i, K, E)}{b_i^{e^3}}. \quad (21)$$

□

G.2. Proof of Lemma 4.2

Lemma 4.2. Let $\Delta_{m,m'}(b^1) := \|\mu_m^*(b^1) - \mu_{m'}^*(b^1)\|$ when $\forall i : b_i^1 = b^1$. The overlap between components $\mathcal{N}(\mu_m^*(b^1), \Sigma_m^*(b^1))$ and $\mathcal{N}(\mu_{m'}^*(b^1), \Sigma_{m'}^*(b^1))$ is $O_{m,m'} = 2Q(\frac{\sqrt{p}\Delta_{m,m'}(b^1)}{2\sigma^1(b^1)})$, where $\sigma^1(b^1) := \text{Var}[\Delta \tilde{\theta}_i^1 | \theta^{init}, b_i^1 = b^1]$ and $Q(\cdot)$ is the Q function. Furthermore, if we increase $b_i^1 = b^1$ to $b_i^1 = kb^1 \leq N$ (for all i), we have $O_{m,m'} \leq 2Q(\frac{\sqrt{kp}\Delta_{m,m'}(b^1)}{2\rho\sigma^1(b^1)})$, where $1 \leq \rho \in \mathcal{O}(1)$ is a small constant.

Proof. We first find the overlap between two arbitrary Gaussian distributions. Without loss of generality, let's assume we are in 1-dimensional space and that we have two Gaussian distributions both with variance σ^2 and with means $\mu_1 = 0$ and $\mu_2 = \mu$ ($\|\mu_1 - \mu_2\| = \mu$), respectively. Based on symmetry of the distributions, the two components start to overlap at $x = \frac{\mu}{2}$. Hence, we can find the overlap between the two gaussians as follows:

$$O := 2 \int_{\frac{\mu}{2}}^{\infty} \frac{1}{\sqrt{2\pi}\sigma} e^{-\frac{x^2}{2\sigma^2}} dx = 2 \int_{\frac{\mu}{2\sigma}}^{\infty} \frac{1}{\sqrt{2\pi}} e^{-\frac{x^2}{2}} dx = 2Q(\frac{\mu}{2\sigma}), \quad (22)$$

where $Q(\cdot)$ is the tail distribution function of the standard normal distribution. Now, let's consider the 2-dimensional space, and consider two similar symmetric distributions centered at $\mu_1 = (0, 0)$ and $\mu_2 = (\mu, 0)$ ($\|\mu_1 - \mu_2\| = \mu$) and with $\Sigma_1 = \Sigma_2 = \begin{bmatrix} \sigma^2 & 0 \\ 0 & \sigma^2 \end{bmatrix}$. The overlap between the two gaussians can be found as:

$$O = 2 \int_{-\infty}^{\infty} \int_{\frac{\mu}{2}}^{\infty} \frac{1}{2\pi\sigma^2} e^{-\frac{x^2+y^2}{2\sigma^2}} dx dy = 2 \int_{\frac{\mu}{2\sigma}}^{\infty} \frac{1}{\sqrt{2\pi}\sigma} e^{-\frac{x^2}{2\sigma^2}} dx \cdot \int_{-\infty}^{\infty} \frac{1}{\sqrt{2\pi}\sigma} e^{-\frac{y^2}{2\sigma^2}} dy = 2Q(\frac{\mu}{2\sigma}). \quad (23)$$

If we compute the overlap for two similar symmetric p -dimensional distributions with $\|\mu_1 - \mu_2\| = \mu$ and variance σ^2 in every direction, we will get to the same result $2Q(\frac{\mu}{2\sigma})$.

In the lemma, when using batch size b^1 , we have two Gaussian distributions $\mathcal{N}(\mu_m^*(b^1), \Sigma_m^*(b^1))$ and $\mathcal{N}(\mu_{m'}^*(b^1), \Sigma_{m'}^*(b^1))$, where

$$\Sigma_m^*(b^1) = \Sigma_{m'}^*(b^1) = \begin{bmatrix} \frac{\sigma^{1^2}(b^1)}{p} & & \\ & \ddots & \\ & & \frac{\sigma^{1^2}(b^1)}{p} \end{bmatrix}. \quad (24)$$

Therefore, from Equation (23), we can immediately conclude that the overlap between the two Gaussians, which we denote with $O_{m,m'}(b^1)$, is:

$$O_{m,m'}(b^1) = 2Q\left(\frac{\sqrt{p}\Delta_{m,m'}(b^1)}{2\sigma^1(b^1)}\right), \quad (25)$$

which proves the first part of the lemma.

Now, let's see the effect of increasing batch size. First, note that we had:

$$\begin{aligned} \Delta\tilde{\theta}_i^1 &= \theta_i^{1,E_i^1} - \theta_i^{1,0}, \\ \theta_i^{1,k} &= \theta_i^{1,k-1} - \eta_l \tilde{g}_i(\theta_i^{1,k-1}), \quad k = 1, \dots, E_i^1, \end{aligned} \quad (26)$$

where $E_i^1 = K \cdot \lceil \frac{N}{b^1} \rceil$ is the total number of gradients steps taken by client i during communication round $e = 1$. Therefore, considering that DP batch gradients are clipped with a bound c , we have:

$$\|\mathbb{E}[\Delta\tilde{\theta}_i^1(b^1)]\| \leq E_i^1 \cdot \eta_l \cdot c. \quad (27)$$

When we increase batch size b_i^1 for all clients from b^1 to kb^1 , the upperbound in Equation (27) gets k times smaller. In fact by doing so, the number of local gradient updates that client i performs during round $e = 1$, which is equal to E_i^1 , decreases k times. As such, we can write:

$$\Delta\tilde{\theta}_i^1(b^1) = k \cdot \Delta\tilde{\theta}_i^1(kb^1) + v_i, \quad (28)$$

where $v_i \in \mathbb{R}^p$ is a vector capturing the discrepancies between $\Delta\tilde{\theta}_i^1(b^1)$ and $k \cdot \Delta\tilde{\theta}_i^1(kb^1)$. Therefore, we have:

$$\begin{aligned} \mu_m^*(b^1) &= \mathbb{E}[\Delta\tilde{\theta}_i^1(b^1)|s(i) = m] = \mathbb{E}[k \cdot \Delta\tilde{\theta}_i^1(kb^1) + v_i|s(i) = m] \\ &= k \cdot \mathbb{E}[\Delta\tilde{\theta}_i^1(kb^1)] + \mathbb{E}[v_i|s(i) = m] = k \cdot \mu_m^*(kb^1) + \mathbb{E}[v_i|s(i) = m]. \end{aligned} \quad (29)$$

Therefore, we have:

$$\|\mu_m^*(b^1) - \mu_{m'}^*(b^1)\| = \left\| k\mu_m^*(kb^1) - k\mu_{m'}^*(kb^1) + \left(\mathbb{E}[v_i|s(i) = m] - \mathbb{E}[v_i|s(i) = m'] \right) \right\|. \quad (30)$$

Based on our experiments, the last term above, in parenthesis, is small and we can have the following approximation for the equation above:

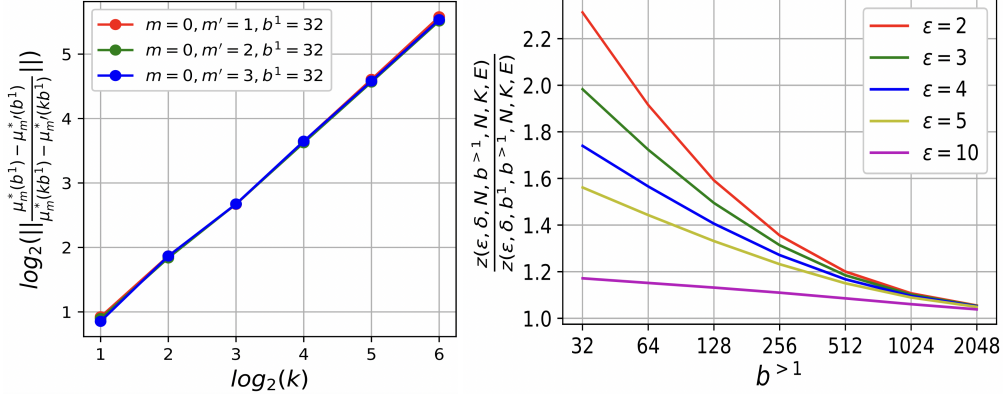


Figure 14. **Left:** Distance between the centers of different clusters, i.e., the distance between $\mu_m^*(b^1)$ and $\mu_{m'}^*(b^1)$, decreases k times as b^1 increases k times. The three curves in the plot are obtained on CIFAR10 with 4 clusters $m \in \{0, 1, 2, 3\}$ obtained from covariate shift (rotation). The curves are overlapping all with slope 0.95, which is very close to 1. This shows the validity of the approximation in Equation (32). **Right:** Effect of changing batch size b^1 to full batch size in the first round on the noise scale z . In the denominator, b^1 is equal to $b^{>1}$. Results are obtained from Renyi-DP accountant (Mironov et al., 2019) with $N = 50000$, $K = 1$ and $E = 200$. For each value of ϵ , we have shown the results for seven values of $b^{>1}$.

$$\|\mu_m^*(b^1) - \mu_{m'}^*(b^1)\| \approx \|k\mu_m^*(kb^1) - k\mu_{m'}^*(kb^1)\|, \quad (31)$$

or equivalently:

$$\|\mu_m^*(kb^1) - \mu_{m'}^*(kb^1)\| \approx \frac{\|\mu_m^*(b^1) - \mu_{m'}^*(b^1)\|}{k}. \quad (32)$$

Figure 14 (left) shows the validity of the approximation above with some experimental results. On the other hand, from Equation (2) and also noting that a client, with dataset size N and batch size b^1 , takes $\frac{N}{b^1}$ gradient steps during each epoch of the first round, we have:

$$\forall m \in [M] : \sigma_m^2(b^1) = \sigma^2(b^1) \approx K \cdot N \cdot \eta_l^2 \cdot \frac{pc^2 z^2(\epsilon, \delta, b^1, b^{>1}, N, K, E)}{b^{1^3}}. \quad (33)$$

When we change the batch size used during the first communication round $e = 1$ from b^1 to kb^1 and we fix the batch size of rounds $e > 1$, then the noise scale z changes from $z(\epsilon, \delta, b^1, b^{>1}, N_i, K, E)$ to $z(\epsilon, \delta, kb^1, b^{>1}, N_i, K, E)$. Confirmed by our experimental analysis (see Figure 14, right), the amount of change in z due to this is small, as we have changed the batch size only in the first round $e = 1$ from b^1 to kb^1 , while the batch sizes in the other $E - 1$ rounds are unchanged and $E \gg 1$. Therefore, supported by the results in Figure 14, we can always establish an upper bound on the amount of change in z as b^1 increases: $z(\epsilon, \delta, kb^1, b^{>1}, N, K, E) \leq \rho z(\epsilon, \delta, b^1, b^{>1}, N, K, E)$, where ρ is a small constant (e.g. $\rho = 2.5$ in Figure 14). So we have:

$$\begin{aligned} \forall m \in [M] : \sigma_m^2(kb^1) &= \sigma^2(kb^1) \approx K \cdot N \cdot \eta_l^2 \cdot \frac{pc^2 z^2(\epsilon, \delta, kb^1, b^{>1}, N, K, E)}{(kb^1)^3} \\ &\leq K \cdot N \cdot \eta_l^2 \cdot \frac{pc^2 \rho^2 z^2(\epsilon, \delta, b^1, b^{>1}, N, K, E)}{(kb^1)^3} \\ &= \frac{\rho^2 \sigma^2(b^1)}{k^3}. \end{aligned} \quad (34)$$

From Equation (32) and Equation (34), we have:

$$O_{m,m'}(kb^1) = 2Q\left(\frac{\sqrt{p}\Delta_{m,m'}(kb^1)}{2\sigma(kb^1)}\right) \leq 2Q\left(\frac{\sqrt{p}\frac{\Delta_{m,m'}(b^1)}{k}}{2\frac{\rho\sigma(b^1)}{k^{\frac{3}{2}}}}\right) = 2Q\left(\frac{\sqrt{kp}\Delta_{m,m'}(b^1)}{2\rho\sigma(b^1)}\right), \quad (35)$$

which completes the proof. \square

G.3. Proof of Theorem 4.3

Theorem 4.3. (Ma et al., 2000) Given model updates $\{\tilde{\theta}_i^1(b^1)\}_{i=1}^n$, as samples from a true mixture of Gaussians $\psi^*(b^1) = \{\mathcal{N}(\mu_m^*(b^1), \Sigma_m^*(b^1)), \alpha_m^*\}_{m=1}^M$, if $O^{\max}(\psi^*(b^1))$ is small enough, then:

$$\lim_{r \rightarrow \infty} \frac{\|\psi^{r+1} - \psi^*(b^1)\|}{\|\psi^r - \psi^*(b^1)\|} = o\left([O^{\max}(\psi^*(b^1))]^{0.5-\gamma}\right), \quad (5)$$

as n increases. ψ^r is the GMM parameters returned by EM after r iterations. γ is an arbitrary small positive number, and $o(x)$ means it is a higher order infinitesimal as $x \rightarrow 0$: $\lim_{x \rightarrow 0} \frac{o(x)}{x} = 0$.

Proof. The proof directly follows from the proof of Theorem 1 in (Ma et al., 2000) by considering $\{\tilde{\theta}_i^1(b^1)\}_{i=1}^n$ as the samples of Gaussian mixture $\{\mathcal{N}(\mu_m^*(b^1), \Sigma_m^*(b^1)), \alpha_m^*\}_{m=1}^M$. \square

G.4. Formal privacy guarantees of R-DPCFL

The privacy guarantee of R-DPCFL for each client i in the system comes from the fact that the client runs DP-SGD with a fixed DP noise variance $\sigma_{i,\text{DP}}^2 = c^2 \cdot z_i^2(\epsilon, \delta, b_i^1, b_i^{>1}, N_i, K, E)$ in each of its batch gradient computations. We provide a formal privacy guarantee for the algorithm to show the sample-level DP privacy guarantees provided to each client i with respect to its local dataset \mathcal{D}_i and against the untrusted server (and any other external third party).

Theorem G.1. The set of model updates $\{\tilde{\theta}_i^e\}_{e=1}^E$, which are uploaded to the server by each client $i \in \{1, \dots, n\}$ during the training time, as well as their local model cluster selections satisfy (ϵ, δ) -DP with respect to the client's local dataset \mathcal{D}_i , where the parameters ϵ and δ depend on the amount of DP noise $\sigma_{i,\text{DP}}^2$ used by the client.

Proof. The sensitivity of the batch gradient in Equation (1) to every data sample is c . Therefore, based on Proposition 7 in (Mironov, 2017) each of the batch gradient computations by client i (in the first round $e = 1$ as well as the next rounds $e > 1$) is $(\alpha, \frac{\alpha c^2}{2\sigma_{i,\text{DP}}^2})$ -RDP w.r.t the local dataset \mathcal{D}_i . Therefore, if the client runs E_i^{tot} total number of gradient updates during the training time, which results in the model updates $\{\tilde{\theta}_i^e\}_{e=1}^E$ uploaded to the server, the set of model updates will be $(\alpha, \frac{E_i^{\text{tot}} \alpha c^2}{2\sigma_{i,\text{DP}}^2})$ -RDP w.r.t \mathcal{D}_i , according to Proposition 1 in (Mironov, 2017). Finally, according to Proposition 3 in the same work, this guarantee is equivalent to $(\frac{E_i^{\text{tot}} \alpha c^2}{2\sigma_{i,\text{DP}}^2} + \frac{\log(1/\delta)}{\alpha-1}, \delta)$ -DP (for any $\delta > 1$). The RDP-based guarantee is computed over a bunch of orders α and the best result among them is chosen as the privacy guarantee. Therefore, the proof is complete and the set $\{\tilde{\theta}_i^e\}_{e=1}^E$ satisfies (ϵ, δ) -DP w.r.t \mathcal{D}_i , with $\epsilon = \frac{E_i^{\text{tot}} \alpha c^2}{2\sigma_{i,\text{DP}}^2} + \frac{\log(1/\delta)}{\alpha-1}$ derived above, and $\delta > 0$. Tight bounds for ϵ can be derived by using the numerical procedure, proposed in (Mironov et al., 2019), for accounting sampled Gaussian mechanism. On the other hand, clients' local cluster selections are also privatized by exponential mechanism and satisfy (ϵ, δ) -DP. Therefore, the overall training process for each client is private and satisfies (ϵ, δ) -DP. \square

H. The relation between Lemma 4.1 and the law of large numbers

We first state the weak law of large numbers and then explain how Lemma 4.1 is closely related to it.

Theorem H.1 (Weak law of large numbers (Billingsley, 1995)). Suppose that $\{X_i\}_{i=1}^b$ is an independent sequence (of size b) of i.i.d random variables with expected value μ and positive variance σ^2 . Define $\bar{X}_b = \frac{\sum_{i=1}^b X_i}{b}$ as their sample mean. Then, for any positive number $\Delta > 0$:

$$\lim_{b \rightarrow \infty} \Pr[|\bar{X}_b - \mu| > \Delta] = 0. \quad (36)$$

In fact, the weak law of large numbers states that the sample mean of some i.i.d random variables converges in probability to their expected value (μ). Furthermore, we can see that $\text{Var}[\bar{X}_b] = \frac{\sigma^2}{b}$, which means that *the variance of the sample mean decreases as the sample size b increases*.

Now, remember from Equation (1) that when computing the DP stochastic batch gradients in round e (with batch size b_i^e), we add DP noise with variance $\sigma_{i,\text{DP}}^2/b_i^e$ to each of the b_i^e clipped sample gradients in the batch *and average the resulting b_i^e noisy clipped sample gradients*. The sampled noise terms added to the clipped sample gradients in a batch are i.i.d with mean zero. Therefore, based on the above theorem, the variance of their average over each batch should approach zero as the batch size b_i^e grows. The same discussion applies to all the $K \cdot N_i/b_i^e$ gradient updates performed by client i during a communication round e (whose noises will be summed up), which results in Lemma 4.1.

I. Gradient accumulation

When training large models with DP-SGD, increasing the batch size results in memory exploding during training or finetuning. This might happen even when we are not using DP training. On the other hand, using a small batch size results in larger stochastic noise in batch gradients. Also, in the case of DP training, using a small batch size results in fast increment of DP noise (as explained in Lemma 4.1 in details). Therefore, if the memory budget of devices allow, we prefer to avoid using small batch sizes. But what if there is a limited memory budget? A solution for virtually increasing batch size is “gradient accumulation”, which is very useful when the available physical memory of GPU is insufficient to accommodate the desired batch size. In gradient accumulation, gradients are computed for smaller batch sizes and summed over multiple batches, instead of updating model parameters after computing each batch gradient. When the accumulated gradients reach the target logical batch size, the model weights are updated with the accumulated batch gradients. The page in https://opacus.ai/api/batch_memory_manager.html shows more details.

J. Further Related Works

Performance parity in FL: Performance parity of the final trained model across clients is an important goal in FL. Addressing this goal, (Mohri et al., 2019) proposed Agnostic FL (AFL) by using a min-max optimization approach. TERM (Li et al., 2020a) used tilted losses to up-weight clients with large losses. Finally, (Li et al., 2020b) and (Zhang et al., 2023) proposed q -FFL and PropFair, inspired by α -fairness (Lan et al., 2010) and proportional fairness (Bertsimas et al., 2011), respectively. Generating one common model for all clients, these techniques do not perform well when the data distribution across clients is highly heterogeneous or a structured data heterogeneity exists across clusters of clients. While model personalization techniques (e.g., MR-MTL (Liu et al., 2022a)) are proposed for the former case, stronger personalization techniques, e.g., client clustering, are used for the latter.

Differential privacy, group fairness and performance parity: Gradient clipping and random noise addition used in DP-SGD disproportionately affect underrepresented groups. Some works tried to address the tension between group fairness and DP in centralized settings (Tran et al., 2020) (by using Lagrangian duality) and FL settings (Pentyala et al., 2022) (by using Secure Multiparty Computation (MPC)). Another work tried to remove the disparate impact of DP on model performance of minority groups in centralized settings (Esipova et al., 2022), by preventing gradient misalignment across different groups of data. Unlike the previous works on group fairness, our work adopts cross-model fairness, where the utility drop after adding DP must be close for different groups (Dwork et al., 2012), including minority and majority clients. As we consider a structured data heterogeneity across clients, the mentioned approaches are not appropriate, due to generating one single model for all.